JOURNAL OF GEOPHYSICAL RESEARCH, VOL. 105, NO. B11, PAGES 25,423–25,450, NOVEMBER 10, 2000

The Australian continental upper mantle: Structure and deformation inferred from surface waves

E. Debayle[1] and B. L. N. Kennett

Research School of Earth Sciences, Australian National University, Canberra

Abstract. We present a new three-dimensional model for the SV wave heterogeneities and azimuthal anisotropy in the upper mantle of the Australasian region. The model is constrained by the waveforms of 2194 Rayleigh waves seismograms with a dense ray coverage that ensure a lateral resolution of the order of few hundred of kilometers. The use of higher modes allows the resolution of the structure down to depths of at least 400 km. In the upper 200 km of the model, seismic velocities are lower on the eastern Phanerozoic margin of the continent compared to the Precambrian central and western cratons, in agreement with previous results for Australia. The boundary between Phanerozoic and Precambrian Australia is not clear, especially in the south, where a broad positive seismic anomaly underlays the Lachlan Fold Belt. The high-velocity lid beneath the continent shows significant variations in thickness. Locally, it may extend down to a depth of 300 km in the mantle, but for most of Precambrian Australia the lithospheric thickness oscillates around 200 km, while it is thinner on the eastern Phanerozoic margin. We found significant SV wave azimuthal anisotropy in the upper 250 km of the mantle, with a drastic change in the organization of anisotropy between the upper 150 km of the model and the deeper part, as revealed in a preliminary inversion. In the upper 150 km of the mantle, azimuthal anisotropy appears more likely to be related to past deformation frozen in the lithosphere, and in central Australia we found clear evidence that deformation is preserved since the Alice Springs orogeny. Below 150 km, a smoother pattern of anisotropy is observed, more likely to be related to present-day deformation due to the northward motion of the Australian plate. Our current data set allows constraint of the anisotropic directions at different depths with an unprecedented lateral resolution. The observation of significant changes of anisotropic directions with depth in the Australian continental mantle suggests that care should be taken in the interpretation of anisotropy from SKS observations.

1. Introduction

Our knowledge of the structure of the upper mantle has improved markedly since the 1970s as the result of improvements in seismological techniques. The early studies of global surface waves [*Dziewonski,* 1971; *Okal,* 1977; *Lévêque,* 1980] were based on an a priori division of the Earth into tectonic provinces and suggested strong correlation between surface tectonics and seismic heterogeneity in the upper 300-400 km of the mantle. The correlation was reinforced by the first tomographic models at the beginning of the 1980s [e.g., *Woodhouse and Dziewonski,* 1984]. In the past 20 years, both the available computational power and the volume of data have increased dramatically, allowing the development of new techniques for imaging the structure as well as a better coverage of the Earth's surface with seismic observations. Higher modes have been included in the analysis of surface wave seismograms [e.g., *Nolet,* 1975; *Cara,* 1978; *Lerner Lam and Jordan,* 1983; *Cara and Lévêque,* 1987; *Nolet,* 1990; *Zielhuis and Nolet,* 1994b; *Stutzmann and Montagner,* 1993; *van Heijst and Woodhouse,* 1997; *van der Lee and Nolet,* 1997a], allowing an increase in the resolution for the transition zone of the upper mantle. With the larger volume of data available, the lateral resolution in global tomographic models has increased to reach 1000 km for the most recent studies [*Zhang and Tanimoto,* 1993; *Trampert and Woodhouse,* 1996]. Upper mantle anisotropy has been observed in many parts of the world, mainly from observations of shear wave splitting [e.g., *Silver and Chan,* 1991; *Vinnik et al.,* 1992; *Tong et al.,* 1994] and the inversion of surface wave data [*Nataf et al.,* 1984; *Tanimoto and*

[1]Now at Institut de Physique du Globe (Centre National de la Recherche Scientifique and Université Louis Pasteur), Strasbourg, France.

Paper number 2000JB900212.
0148-0227/00/2000JB900212$09.00

Anderson, 1984; *Montagner and Tanimoto,* 1990, 1991]. This upper mantle anisotropy is commonly attributed to the lattice preferred orientation (LPO) of anisotropic minerals, especially olivine, which displays a strong intrinsic anisotropy and is abundant in the upper mantle. Oriented olivine models are usually compatible with seismic observations, and much evidence for olivine orientation in upper mantle fabrics has been observed [e.g., *Pelsenick and Nicolas,* 1978; *Christensen and Salisbury,* 1979].

We have now a seismic picture of the upper mantle refined by many regional and global studies, which can be broadly described as follows: For oceanic areas, the pattern of seismic heterogeneities and anisotropy is largely dominated by the cooling of the oceanic plates as they move away from the ridge axis. The lithosphere is generally well characterized by a high-velocity lid whose thickness increases from 30 to 75-100 km with the age of the seafloor [e.g., *Forsyth,* 1975; *Nishimura and Forsyth,* 1989]. The lithosphere is underlain by a low-velocity layer, the asthenosphere, where partial melting is likely to occur. Polarization anisotropy inferred from the discrepancy in dispersion between Love and Rayleigh waves is generally found in the first 300 km of the upper mantle [*Cara and Lévêque,* 1988; *Nishimura and Forsyth,* 1989; *Lévêque et al.,* 1998]. Azimuthal anisotropy has been observed in the Pacific, Indian, and Atlantic Oceans [*Forsyth,* 1975; *Nishimura and Forsyth,* 1989, *Montagner,* 1986b; *Roult et al.,* 1987; *Montagner and Jobert,* 1988; *Lévêque et al.,* 1998, *Silveira et al.,* 1998] and at a global scale [*Tanimoto and Anderson,* 1984; *Montagner and Tanimoto,* 1990, 1991]. Such azimuthal anisotropy generally displays strong correlation at asthenospheric depth with the absolute motion of oceanic plates. This has been used as a strong argument to invoke a significant contribution of asthenospheric deformation induced by current plate motion to oceanic anisotropy. In the lithosphere, surface wave data favor a frozen anisotropy reflecting the way in which the lithosphere has been emplaced [e.g., *Nishimura and Forsyth,* 1989; *Lévêque et al.,* 1998].

The continental upper mantle has a more complex seismic structure, which reflects its long history. Generally, high seismic velocities are found beneath the oldest Precambrian cratons, while the more recent Phanerozoic regions display lower velocities [*Zielhuis and Nolet,* 1994a; *Zielhuis and van der Hilst,* 1996; *van der Lee and Nolet,* 1997b], but the depth extent of these continental high-velocity anomalies is still controversial. *Jordan* [1975] used observations of *ScS* travel times and free oscillations to propose that a thick layer of anomalous mantle underlays old continental cratons down to 400 km depth. This would be consistent with most of the global upper mantle tomographic models where high velocities beneath cratons apparently extend to 350 km [e.g., *Woodhouse and Dziewonski,* 1984]. However, significant vertical smearing of such anomalies may be present. Recently, *Ricard et al.* [1996] have shown that the dispersion of fundamental mode Love and Rayleigh waves in the period range 70-200 s is well represented by the a priori 3SMAC model of *Nataf and Ricard* [1996] in which the lithosphere is never thicker than 300 km.

If the lithosphere thickens gradually with age, a thickness of 250 km has been predicted for Archæan cratons [*Fleitout and Yuen,* 1984]. The existence of thicker continental roots would require the presence of compositional heterogeneities in the mantle. Whatever the process invoked, the formation of a thick continental root needs a long period of time, during which the "tectosphere" of *Jordan* [1975] has to translate coherently with plate motion. If thick continental roots move with the plates, shearing between the tectosphere and the underlying mantle is expected deep in the mantle, at the base of the tectosphere with a consequent potential for anisotropy. A major component of anisotropy would be expected in the continental lithosphere, owing to the presence of highly anisotropic minerals, which are likely to have been intensely deformed during a long tectonic history.

In this paper, we investigate azimuthal anisotropy and lateral heterogeneities beneath the Australasian region. We focus on the upper mantle structure beneath Australia, a continent which has experienced a long tectonic history since the Archæan. The continent is the result of the assemblage of numerous fragments of continental crust by plate tectonic processes, which are expected to have left a lasting imprint on the lithospheric mantle. Two thirds of the Australian crust is Precambrian, while the remaining third has been accreted during the Paleozoic [e.g., *Myers et al.,* 1996]. Precambrian Australia comprises three main tectonic units: the northern, western, and southern cratons. The western craton has been accreted from two main Archæan blocks, the Pilbara and Yilgarn cratons, well exposed in western Australia (Figure 1). The northern and southern Australian cratons are probably the results of the assemblage of Proterozoic and Archæan crustal fragments. There is, for example, evidence of Archæan basements within the Pine Creek fragment in northern Australia and the Gawler craton in southern Australia. The three main tectonic units were probably cratonized by 1830 Ma and assembled in a single piece between 1300 and 1100 Ma, as an early component of the Rodinian supercontinent [*Myers et al.,* 1996]. The successive accretion of continental terranes on the eastern margin of the Proterozoic cratons during Paleozoic times has had the effect of shaping the Australian continent to its current form.

In order to resolve anisotropic structure at the scale of the continental blocks which have formed Australia, lateral resolution of the order of few hundred kilometers is required. Within Australia such resolution cannot be achieved with current sparse shear wave splitting studies, although *Clitheroe and van der Hilst* [1998] have assembled results from both portable and permanent stations. The directions of azimuthal anisotropy be-

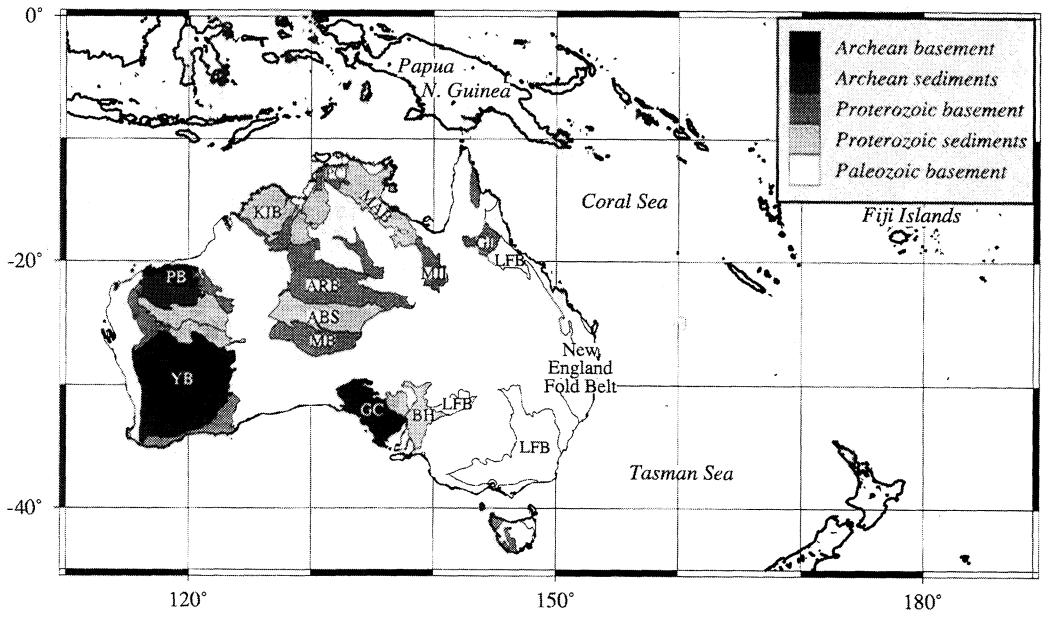

Figure 1. Main geological outcrops of Australia; YB, Yilgarn Block; PB, Pilbara Block; GC, Gawler craton; ARB, Arunta Block; MB, Musgrave Block; BH, Broken Hill Block; MII, Mount Isa Inlier; GI, Georgetown Inlier; PCI, Pine Creek Inlier; KIB, Kimberley Basin; ABS, Amadeus Basin; MAB, McArthur Basin; LFB, Lachlan Fold Belt.

neath continents have been derived from the azimuthal variation of Love and Rayleigh waves on a global scale [*Tanimoto and Anderson,* 1984; *Montagner and Tanimoto,* 1990, 1991] but the lateral resolution in these studies is still not sufficient to draw relevant conclusions at lithospheric depths at a regional scale. *Gaherty and Jordan* [1995] have used both surface wave and body wave observations along one corridor crossing the Australian continent and found significant polarization anisotropy within the lithosphere in the upper 250 km of the Earth but not beneath.

The deployment of portable seismometers over the Australian continent during the Skippy experiment [*van der Hilst et al.,* 1994] allows the use of surface wave data to investigate anisotropic structure with a much finer resolution. *Debayle* [1999] has presented preliminary results for azimuthal anisotropy in the Australian upper mantle from waveform analysis of the fundamental and higher modes of 668 Rayleigh waves seismograms. This preliminary inversion revealed a simple pattern of anisotropy at 150 km depth, with a dominant north-south component close to the present-day absolute plate motion. In this paper, we present a full three-dimensional (3-D) tomographic model which is constrained by a much larger data set recorded by the permanent Incorporated Research Institutions for Seismology (IRIS) and Geoscope stations in the Australian region, supplemented by records from the deployment of portable instruments across Australia during the Skippy experiment and subsequently in the Kimberley region, Western Australia (Kimba experiment). The 3-D shear wave speed model is constructed from the waveform analysis of 2194 Rayleigh wave seismograms using the same procedure as used by *Debayle* [1999]. The use of higher modes from intermediate and deep events allows the structure to be constrained down to at least 400 km depth. The density of path coverage and azimuthal distribution of paths is excellent in central and eastern Australia. As a result, changes in azimuthal anisotropy can be resolved with horizontal wavelengths of few hundred of kilometers, matching the scale of the blocks which coalesced to form the Australian continent. The present study is thus able to provide information to supplement both previous azimuthal anisotropy maps obtained from surface wave data with a much poorer lateral resolution [e.g., *Montagner and Tanimoto,* 1991; *Lévêque et al.,* 1998] and teleseismic shear wave observations, which have provided sparse measurements of fast S wave directions with an excellent lateral but a poor vertical resolution [e.g., *Clitheroe and van der Hilst,* 1998; *Vinnik et al.,* 1992]. The results also complement the earlier work of *Zielhuis and van der Hilst* [1996] and *van der Hilst et al.* [1998] for the Australian region by providing a new 3-D upper mantle model for SV velocity obtained from a larger data set with a different inversion method.

2. Inversion Procedure

Our object is to produce a 3-D model of shear wave speed together with the distribution of azimuthal anisotropy. The approach we have used is similar to the work of *Nolet* [1990], by having two distinct stages with different style of inversion but different algorithms are used in each step.

The first part of the inversion consists of an analy-

sis of individual seismograms. With the aid of a source model we find a radially stratified model associated with the path from source to receiver for which synthetic seismograms match the observations. The 1-D upper mantle model is constructed using the technique developed by *Cara and Lévêque* [1987] (hereinafter referred as CL) applied to the surface wave segment of the seismogram comprising the fundamental Rayleigh mode and several overtones. The seismograms have been processed using the automated procedure developed by *Debayle* [1999] based on the CL technique.

The 1-D models for each path represent an average of the slowness structure encountered along the path, and so a 3-D model can be built from a linear inversion procedure. *Lévêque et al.* [1998] have shown how this approach can be extended to extract information on azimuthal anisotropy for those regions where there are sufficient crossing paths. The 3-D tomographic model for both the isotropic component of the SV wave speed heterogeneity and the variation in azimuthal anisotropy has been constructed using the continouous regionalization algorithm of *Montagner* [1986a].

The approach adopted in this paper differs from the "partitioned waveform inversion" scheme used by *Zielhuis and van der Hilst* [1996] and *van der Hilst et al* [1998] in previous studies on the Australian region: first, through the use of CL method for the waveform inversion step, and second, in the way in which the inversion for 3-D structure is undertaken. Rather than using a block model we have used a continous representation of the wave speed structure. We have also interpreted the average models as a path average of shear wave slowness rather than shear wave velocity because this leads to a more direct relation to phase slowness (see Appendix A).

3. Waveform Fitting

One of the most difficult aspects of waveform inversion is the highly nonlinear dependence of the recorded signal upon the model parameters. In the CL technique this nonlinearity is reduced through the definition of "secondary observables" constructed from the seismograms prior to inversion. As in the work by *Lerner Lam and Jordan* [1983], cross correlation with modal synthetics is used to reinforce the contribution of a given mode to the signal. The secondary observables are then based on the envelope of these cross-correlogram functions filtered at different frequencies. The concept is close to the isolation filter technique of *Gee and Jordan* [1992]. This waveform inversion technique is described in detail by *Cara and Lévêque* [1987] and *Lévêque et al.* [1991]. The CL procedure minimizes the dependence of the model obtained from the inversion on the starting model, and this enabled *Debayle* [1999] to develop an automated process in which all the various observed seismograms are matched starting with a single initial upper mantle model with a path-dependent crustal model superimposed.

3.1. Data Set

We use the Rayleigh wave portion of seismograms from regional events recorded on permanent and portable broadband recorders. The events occur mainly in the major earthquake belt to the north and east of Australia, from Indonesia through to Fiji and New Zealand, and to a lesser extent from the mid-ocean ridge, between Australia and Antarctica (Figure 2). The permanent stations are those of the IRIS and Geoscope network in the Australasian area. These stations are supplemented by field deployments of portable recorders over the Australian continent, started in 1993 by the Research School of Earth Sciences, Australian National University. Most of the paths crossing the Australian continent correspond to events recorded by networks of up to 12 portable recorders, deployed in the field for up to 6 months at a time, during the Skippy experiment [*van der Hilst et al.*, 1994] and a more recent field deployment in the Kimberley region from July to October 1997 (Kimba). The field instruments are Güralp CMG-3ESP seismometers with a flat velocity response over a frequency band below 30 Hz. Four seismometers have a flat response to 0.016 Hz (62.5 s period) (type 1), while for the remaining eight the flat response extends to 0.033 Hz (30 s period) (type 2). In order to enhance lower-frequency signals, the data are deconvolved using the true instrument response and then reconvolved with a new transfer function having a broader bandwith at long periods. The new transfer functions have been designed to enhance the signal up to 240 s period for instrument of type 1 (Figure 3a), and up to 120 s period for instruments of type 2 (Figure 3c). For longer periods, where the dynamic range of the acquisition system may be insufficient, the signal is suppressed. The waveform inversion is then performed to minimize the difference between the reprocessed records and the synthetics convolved with the appropriate modified instrument response.

3.2. Assumptions in Analysis

The representation of the seismograms in terms of a 1-D averaged model is based on a set of approximations of the character of surface wave propagation in laterally varying media. The frequency range used for the analysis is chosen so that these approximations are justified.

The principal assumption is that the observations can be represented in terms of a multimode surface wave train in which the modes propagate independently without interaction. This approximation is valid for a medium in which the seismic parameters vary smoothly with no strong velocity gradients [*Woodhouse*, 1974]. In this case the propagation characteristics of each mode are governed by the vertical structure beneath each point of the propagation path. The incremental phase for the mode along the path is then simply the integral of the phase slowness along the path, while the path itself is determined by the lateral variations in phase velocity. For longer-period waves it is a reasonable ad-

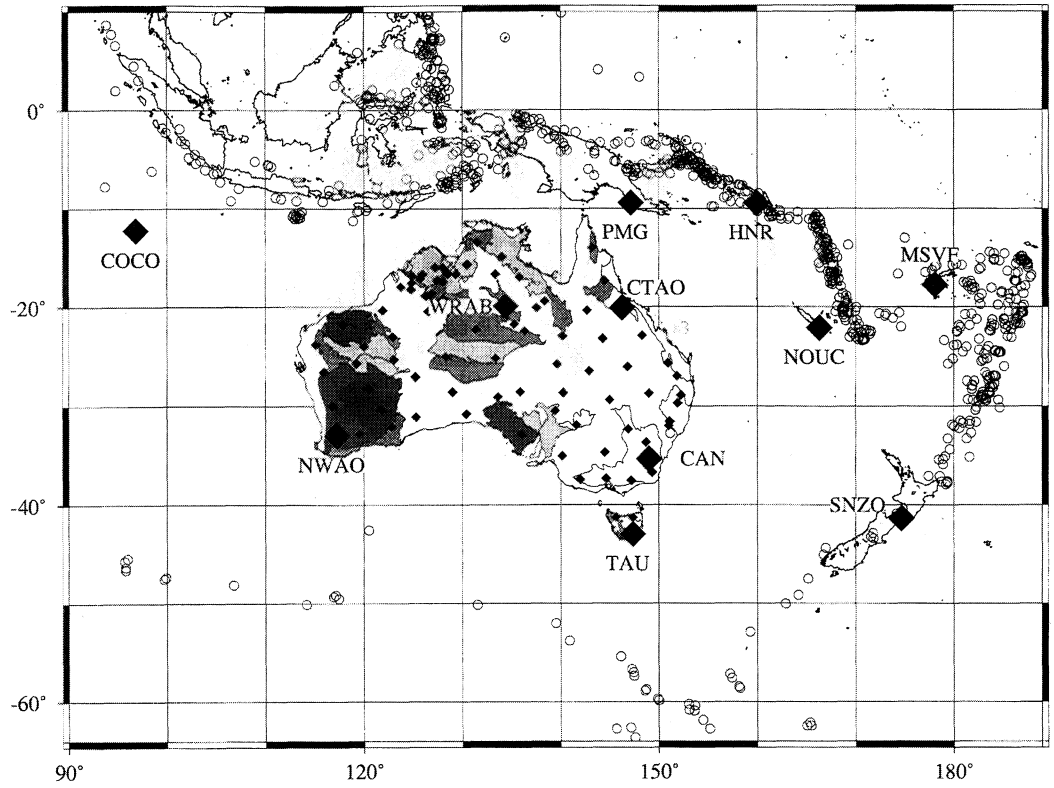

Figure 2. Location of events (open circles) and stations (diamonds) used in this study. Small diamonds indicate portable stations deployed on the field. Large diamonds correspond to the permanent stations from the IRIS and Geoscope networks. The names of the permanent stations are indicated on the display. Geological outcrops are in background.

ditional approximation to neglect the deviations of the path from the great circle between source and receiver since the propagation paths are not very long (normally < 4000 km). Ray tracing in the models obtained from tomographic inversion indicates that while deviations from great circle paths are small at 40 s period for fundamental mode Rayleigh waves, they rapidly become significant as the frequency increases and by 20 s period are also noticeable for higher modes. In addition, the most significant deviation from the great circle appears to be associated with the transition from the Australian continent to the Tasman and Coral Seas for north-south paths grazing the continent edge. Such paths are not recorded at any of the sites we have used.

When we are able to use the path average and great circle approximations, the computation of the synthetic seismogram can be simplified by using a 1-D radially stratified structure for the path. The inversion is performed for a 1-D upper mantle structure, which matches the waveform of the observed seismogram, assuming that the crustal structure and the source excitation are known. The 1-D models derived from the inversion can then be regarded as an average of the local properties along the great circle path [*Nolet,* 1990; *Debayle,* 1996]. As a result, we can undertake a second linear inversion to recover the 3-D structure from the set of averages along the paths.

The great circle approximation provides a simple theoretical framework for the efficient analysis of large volume of data using current work stations. However, in the Australian region we have to recognize that the sources and receivers generally lie on different structures, resulting in paths sampling different tectonic provinces with major transitions such as ocean-continent boundaries. *Kennett* [1995] has explored the validity of the assumptions used for propagation at regional-continental scales where path lengths would typically be between 1000 and 4000 km and concludes that the great circle approximation should normally be suitable for periods between 30 and 100 s. The upper limit is due to the strong lateral heterogeneities present in the upper part of the mantle. The lower limit depends on the path-averaged approximation and on the far-field assumptions made in the computation of source excitation. *Kennett* [1995] also notes that the apparent source contribution is not confined to the immediate neighborhood of the epicenter. Thus, although the source excitation computation can be improved by using a local structure adapted to the source region, the difference between the structures used for the epicenter region and for the propagation path should not be too large, and a difference in crustal thickness that does not exceed 10 km is recommended.

In this study, the seismograms have been analyzed

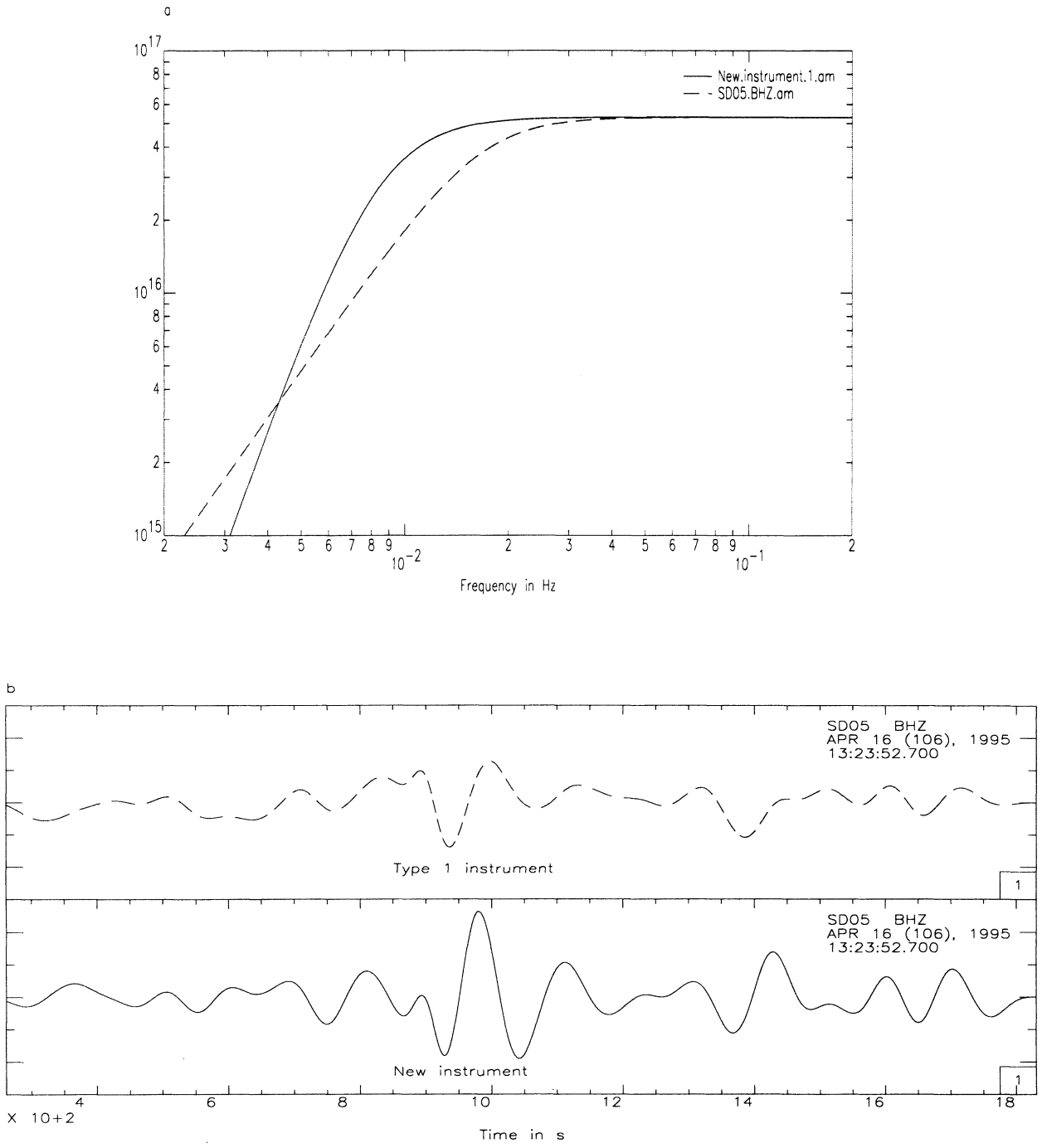

Figure 3. Instrumental response defined for this study (solid line) superimposed in the original Güralp instrument responses (dashed line) for (a) type 1 and (c) type 2 instruments. The new filter enhances the records up to 4.16 mHz (240 s) for type 1 instruments and up to 8.33 mHz (120 s) for type 2 instruments, while at larger period the signal is suppressed. (b and d) Two seismograms as recorded with the original Güralp instrument (dashed line) and reprocessed with the new instrument (solid line). The seismograms are low-pass filtered at 100 s on Figure 3b and 80 s on Fig. 3d to show the effect of the new filter in the bandwidth where it enhances the signal.

using a single upper mantle model for all paths which is a smoothed version of the Preliminary Reference Earth Model (PREM) model [*Dziewonski and Anderson,* 1981], with a crustal model adapted to the path. For each source-receiver pair an averaged crustal model is constructed by taking the crustal part of the 3SMAC model [*Nataf and Ricard,* 1996] averaged along the great circle path. The source excitation is computed for a point double couple following *Cara* [1979], with source parameters taken from the centroid moment tensor solutions determined by Harvard University and published by the National Earthquake Information Service

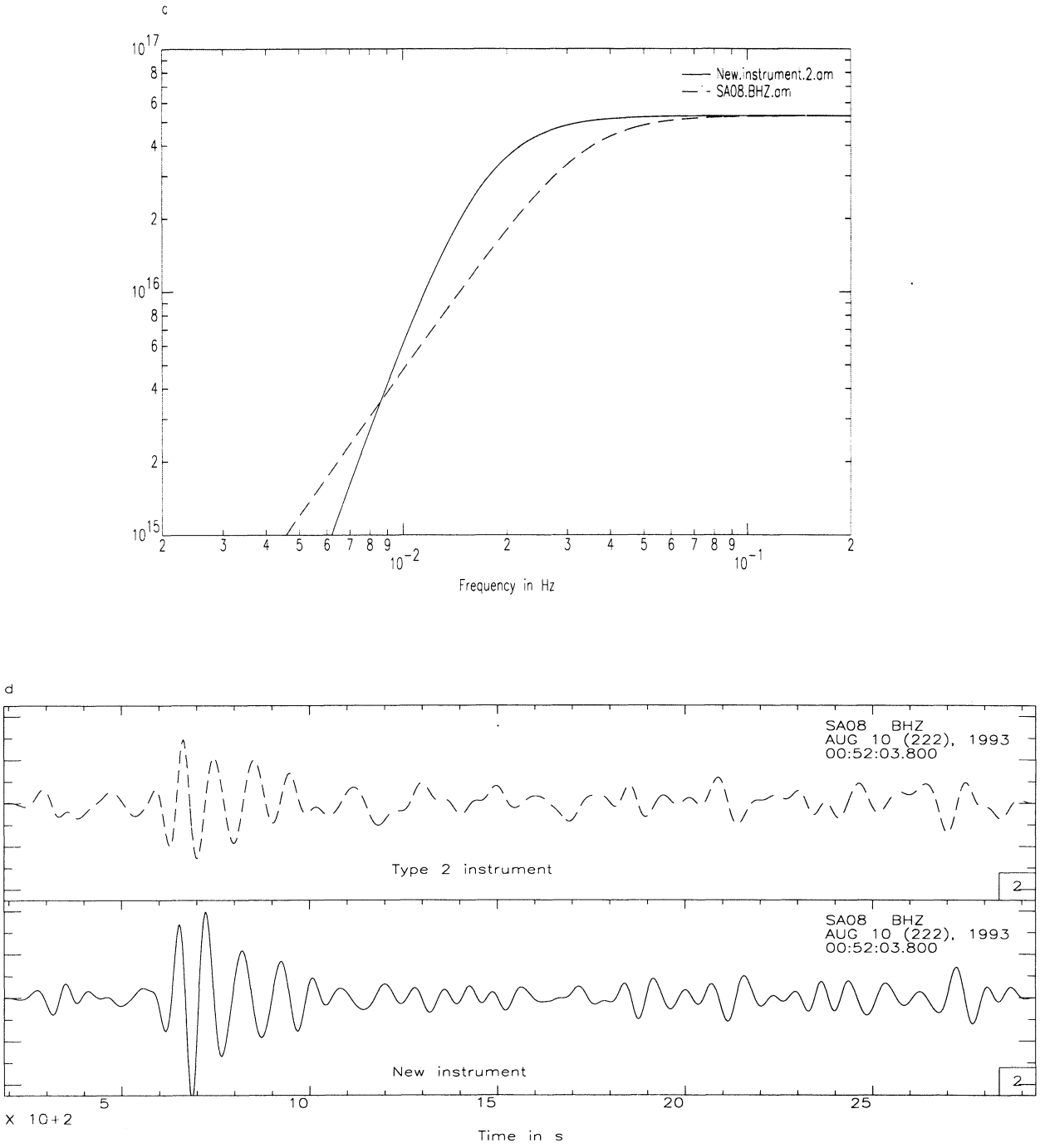

Figure 3. (continued)

(NEIS). The structure used to compute the source excitation for each earthquake is determined by the 3SMAC model in the epicenter region.

For the present data set the largest differences between the crustal structures near the source and path average occur for earthquakes located on the East Indian Ridge recorded on the northern part of the Australian continent or in Papua New Guinea. For these events the crust is generally 7 km thick beneath the East Indian Ridge, and the average crustal thickness along the path does generally not exceed 25 km because a significant part of the propagation is oceanic. The number of events subject to these differences is small, just 9 of the 2194 analyzed, because of the low seismicity of the East Indian Ridge compared to the subduction zones to the north and east of the continent. It is thus likely that crustal thickness differences much larger than 10 km are confined to a small proportion of our data. In addition, we have restricted the upper frequency limit to minimize the influence of lateral heterogeneity and have not used periods shorter than 40 s for both the fundamental and the higher modes. At low frequency, when the quality of the signal was good, we have extended the analysis to longer periods than 100 s, sometimes up to

160 s. However we introduced two safeguards in the automated process: we do not analyze paths shorter than 1000 km and we invert a seismogram at a given period only if the epicenter-station distance is larger than 3 times the wavelength for the period. These choices ensure that the station lies in the far field of the source and that the frequency range is such that the great circle approximation should be valid. Of the 2194 seismograms considered, 188 have been inverted up to 120 s and 275 up to 160 s. The remaining data are inverted in the frequency range 40-100 s.

For the higher-mode component of the wave field we also need to consider the issues of independent mode propagation. Body waves phases are built up from the summation of higher modes but are sensitive to model perturbations close to their geometrical ray rather than to the horizontally averaged model perturbation used in the path-averaged approximation. For higher frequencies the inclusion of mode coupling between surface waves allows an improved representation of the propagation of body waves [*Li and Tanimoto,* 1993; *Marquering and Snieder,* 1995], and the significance of such a scheme in waveform inversion has been recently studied by *Marquering et al.* [1996]. They use a large number of modes (up to 20) to generate synthetic seismograms and perform tests with and without mode coupling using the partitioned waveform inversion of *Nolet* [1990]. They conclude that the neglect of mode coupling does not affect the upper part of the model, which is sampled by the fundamental mode and the first few higher modes. However, at larger depth between 400 and 500 km, significant artefacts can be introduced with limited path coverage. Such effects can be exaggerated when the fundamental mode and higher mode parts of the seismogram are separated in the waveform inversion, with the object of reducing the dominance of the fundamental mode.

In our implementation of the CL method we undertake a simultaneous fit to the fundamental mode and the overtones, and a suitable choice of secondary observables allows information for each mode to be exploited. We have used up to four overtones to compute the synthetic seismograms and perform the waveform inversion. This should minimize the bias due to the neglect of mode coupling, while keeping a good sensitivity in the upper 400 km of the mantle: at 40 s period and in the distance range considered (1000-6000 km), four overtones are adequate to build the *SSS* wave, which samples the upper 400 km of the mantle.

3.3. Selected Examples

Examples of automated waveform inversion for selected paths sampling the main tectonic provinces of Australia are presented in Figures 4, 5, 6, and 7. The paths are shown in Figure 4, and the waveform fit between the observed and computed seismograms is presented prior to the inversion in Figure 5, and after the CL inversion in Figure 6. Figure 7 shows the path-averaged upper mantle shear velocity models determined from the waveform inversion superimposed in the initial model. A good waveform fit is generally achieved for the fundamental mode and the first few overtones (Figure 6) of the real seismograms, even where there are significant differences in waveforms prior to inversion (see paths 2, 11, or 12 in Figure 5, for example). For central and western Australia (all paths except 5, 6, 9, and 12) the path-averaged shear velocity models show a high-velocity lid generally around 200 km thick, underlain by a low-velocity layer (Figure 7). For these data the high-velocity lid is required to fit the fundamental mode of the seismograms, as the initial model predicts synthetics too slow compared to the observed seismograms (Figure 5). Because higher modes are sensitive to both shallow and deep structure, the delay time between synthetics and real higher mode waveforms cannot be simply related to mantle perturbations. However, it remains small compared to the one observed for the fundamental mode, and for most of our data set in central and western Australia, a simultaneous fit of the fundamental and higher modes requires the presence of a slight low-velocity zone below the lid.

Generally, the shear velocity models obtained for neighbouring paths are similar, but differences do occur. An extreme example is presented in Figure 7 for paths 7 and 8. For these two paths the average shear velocity models present similar shapes, but the amplitudes of the perturbations differ significantly in the uppermost 200 km with faster shear velocities for path 8. This can mainly be attributed to the presence of the Banda arc. Path 8 corresponds to an event located in the subduction zone at 69.7 km depth so the path samples the slab for a significant proportion of its length. Path 7, related to a shallower event (15 km), is located to the east and misses the main effect of the slab. While very close, the two paths sample heterogeneous structure, and this is reflected in the recorded waveforms that look rather different as well as in the inverted shear velocity structure. Other effects such as error in the location and depth of the earthquake can also map in the inverted velocity models and contribute to differences between neighboring paths. If there is no objective way to correct for these errors, we can at least try to minimize their effect by favoring a smooth model in the tomographic inversion. Thus, if errors in the source function estimation produce differences between neighboring paths, we expect these differences to be averaged in the tomographic inversion and thus to contribute to the misfit.

Earlier studies revealed a contrast in wave speed between the eastern margin of the continent and its central and western parts. This can be directly observed on our path-averaged velocity models: a noticeable low-velocity zone centered at around 140 km depth characterizes path 12, which samples eastern Australia. Paths 5 and 6 show structures in the uppermost 200 km,

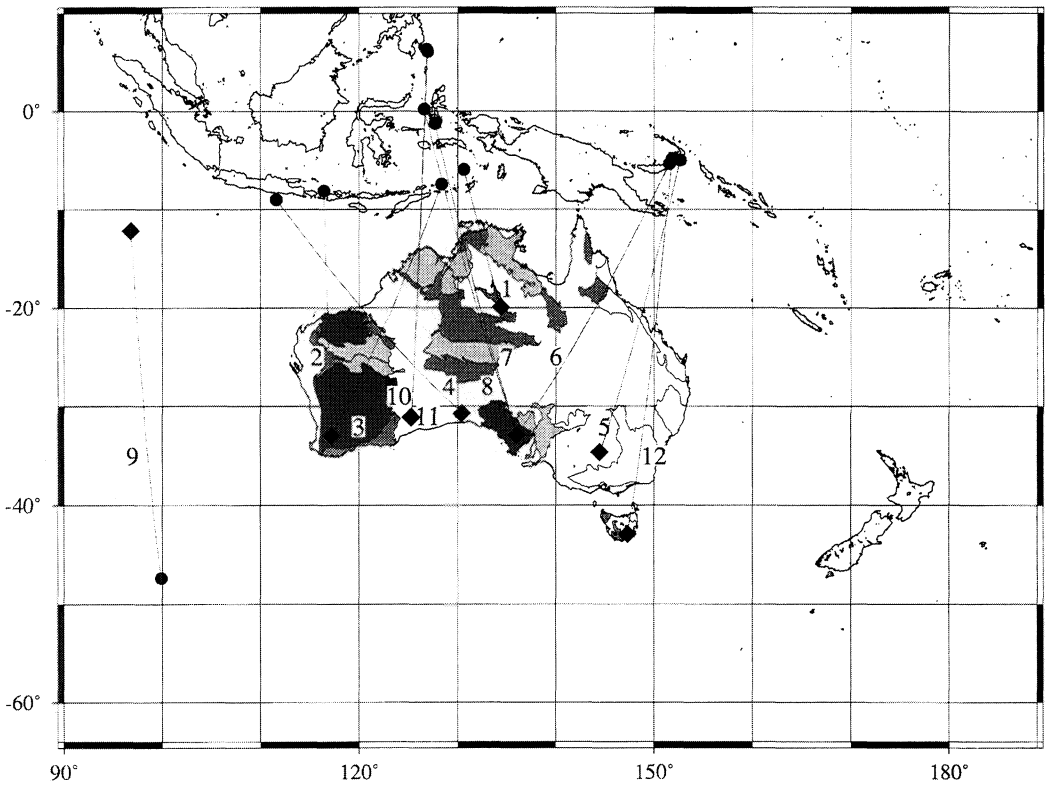

Figure 4. Epicenter-station paths for which the waveform fit and the path-averaged velocity models are shown on Figures 5, 6, and 7. Epicenters are shown with circles; stations are shown with diamonds. Geological outcrops are used as the background.

which are intermediate between the low velocities of the eastern margin and the high velocities of central Australia, probably indicating that they sample heterogeneous structures. Finally, path 9 samples the Indian Ocean basins from the East Indian Ridge to the old oceanic Warton basin. The velocity model for path 9 resembles the P7 model of *Cara* [1979] for the Pacific Ocean. The character of the suite of velocity models in Figure 7 suggests that the main differences between structure in oceanic and continental regions are to be found in the uppermost 200 km of the mantle.

3.4. Path Coverage

The application of our waveform inversion procedure to the Skippy, Kimba, Geoscope, and IRIS data set has resulted in the successful analysis of 2194 Rayleigh wave seismograms corresponding to the path coverage of Figure 8. In the automated process, modes were included in the inversion when they contributed more than 1% of the energy in the seismogram at the requisite period. For the 2194 paths the fundamental mode and at least one overtone have been included for 1193 data (Figure 8a). For 908 paths (Figure 8c) the overtones were poorly excited, and only the fundamental mode was inverted. These data correspond mainly to shallow earthquakes and include almost all the events from the Southeast Indian Ridge. The inversion has been restricted to the higher modes for a limited number of paths (93 paths, Figure 8b) corresponding to deep events for which the fundamental mode could be neglected.

The simultaneous use of fundamental and higher mode information for the 1193 paths of Figure 8a ensures good resolution in the uppermost 400 km of the mantle for most of the Australian continent. The 908 paths of Figure 8c provide additional coverage for the uppermost 250 km, while the 93 paths of Figure 8b help to constrain the deep structure. However, for higher latitudes (below 40°S) our coverage consists mainly of fundamental mode data, and the structural estimate is likely to suffer from a lack of resolution below 250 km depth.

4. The 3-D Model

4.1. Construction

The result of the waveform inversion is that for each path we have a SV wave speed model as a function of depth alone, which matches the observed waveforms of the Rayleigh waves. We now combine the set of 1-D velocity models into a single 3-D model for the lateral variations in shear wave velocity and its azimuthal anisotropy. For this purpose, we use the continuous regionalization algorithm of *Montagner* [1986a]. This algorithm was originally designed for the regionalization

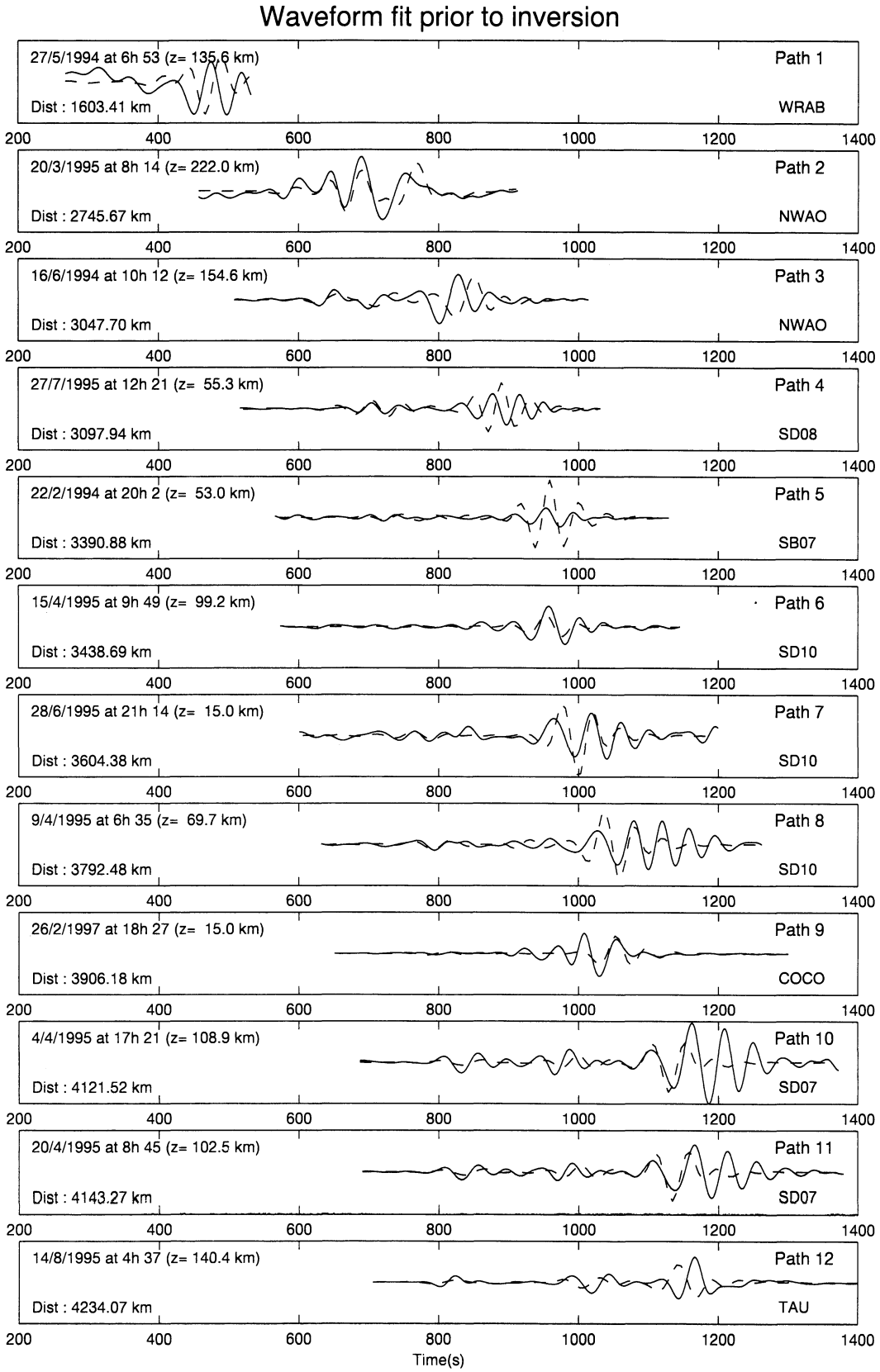

Figure 5. Examples of waveform fit prior to inversion for the 12 paths (data 1 to 12) labeled on Figure 4. Synthetics are in dashed lines, real waveforms are shown with solid lines. Data are ordered by epicentral distance; z is the depth and the station code is given on the lower left corner.

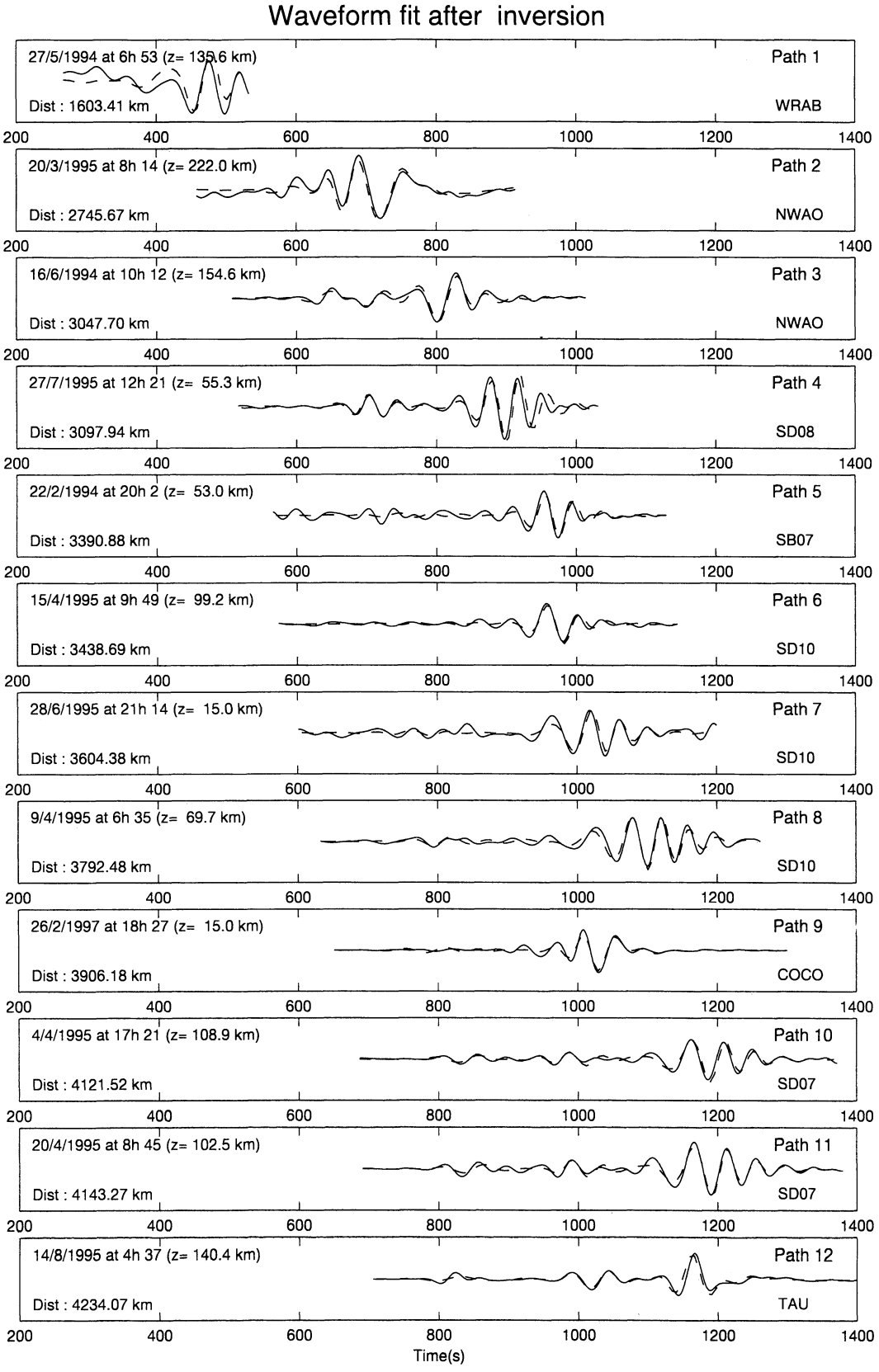

Figure 6. Same as Figure 5 but after inversion.

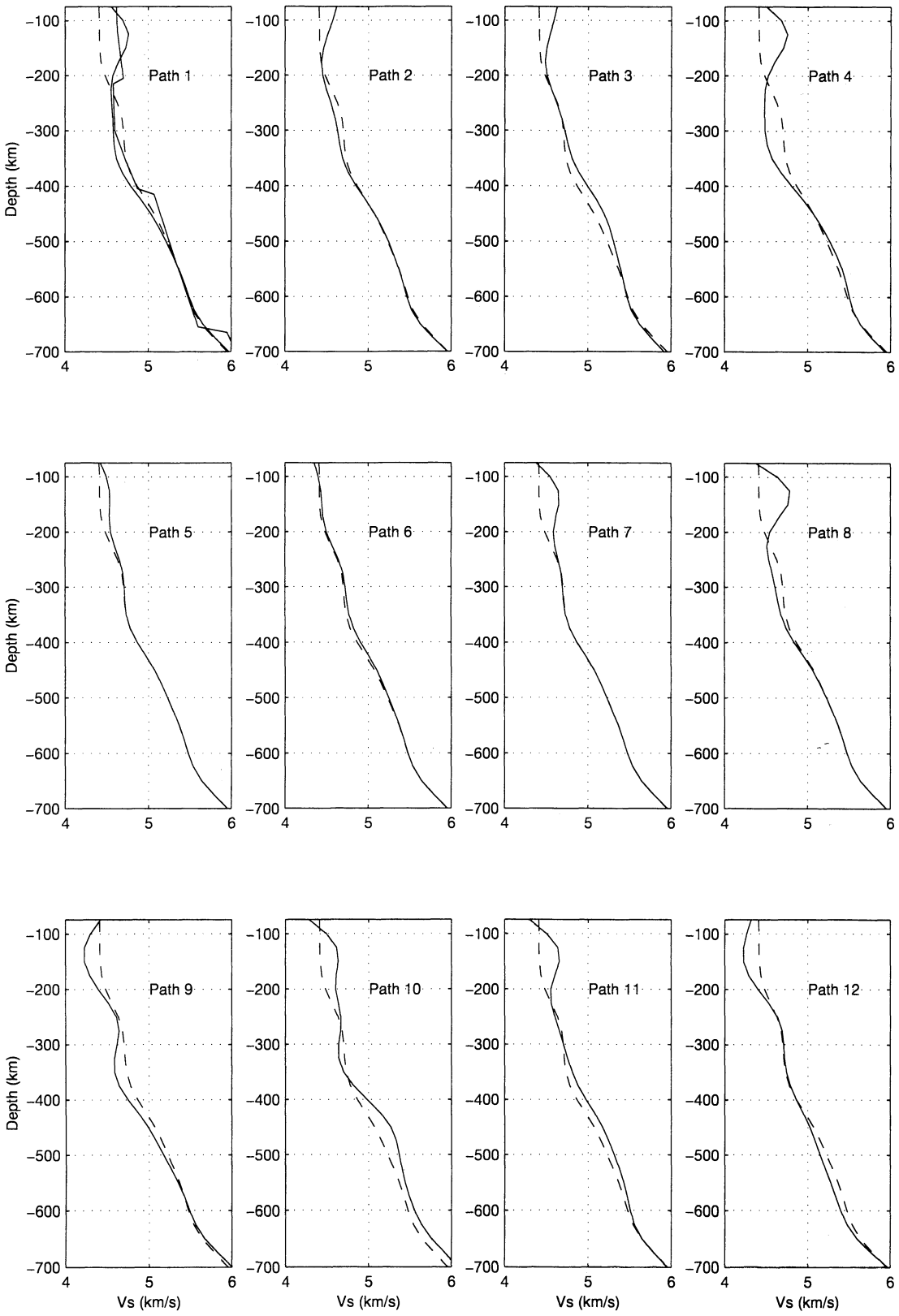

Figure 7. Path-averaged SV velocity models for the 12 data of Figures 5, and 6. The starting upper mantle model for all paths is shown with a dashed line. The model obtained after inversion is shown with a solid line. For path 1 the smooth model is the result of the inversion, and the other is the S wave model of *Kennett et al.* [1994] for northern Australia.

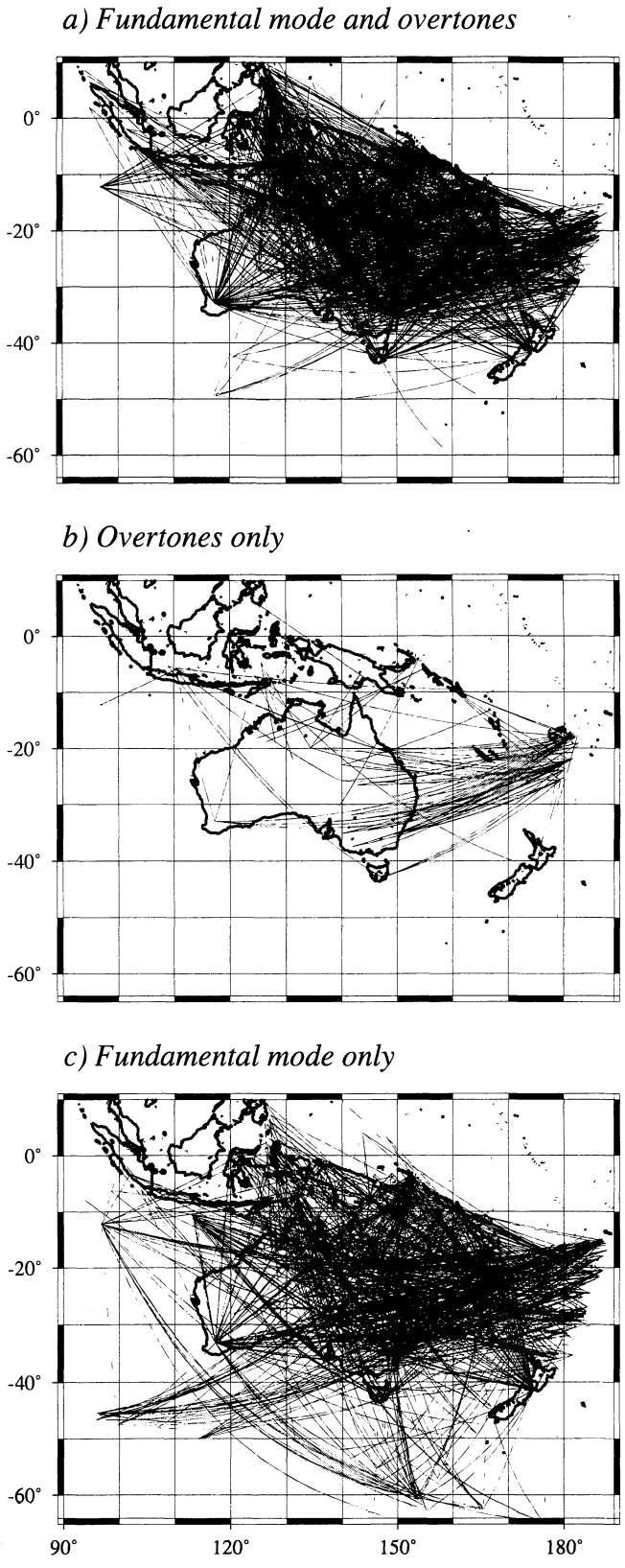

Figure 8. (a) The 1193 paths for which the fundamental mode and at least one overtone have been used in the automated inversion; (b) 93 paths for which only the overtones have been used; and (c) 908 paths for which only the fundamental mode was inverted.

of phase or group velocities at different periods under the assumption that surface waves propagate along the great circle and the propagation time is simply the integral of the phase slowness along the path at period T:

$$\frac{1}{C^{\mathrm{es}}(T)} = \frac{1}{L^{\mathrm{es}}} \int_{\mathrm{es}} \frac{1}{C^{\mathrm{loc}}(T)}\, ds, \tag{1}$$

where L^{es} is the length of the epicenter-station path, C^{es} is the observed phase velocity, and C^{loc} is the local phase velocity at each point along the path. As noted by *Lévêque et al.* [1998], the shear slowness of the 1-D models obtained from the waveform inversion can be regarded as the average of the shear slowness structure along the great circle path between source and receiver (see also Appendix A):

$$\frac{1}{\beta^{\mathrm{es}}(z)} = \frac{1}{L^{\mathrm{es}}} \int_{\mathrm{es}} \frac{1}{\beta^{\mathrm{loc}}(z)}\, ds. \tag{2}$$

The regionalization algorithm of *Montagner* [1986a] can therefore be directly applied to our data set to retrieve the local shear slowness and hence shear wave speed.

Let us now examine how azimuthal anisotropy can be retrieved in the regionalization step. The azimuthal dependence of the local phase and group velocity for Love and Rayleigh waves in a slightly anisotropic medium is given by *Smith and Dahlen* [1973] as the sum of azimuthal and nonazimuthal terms. *Montagner and Nataf* [1986] have shown that the azimuthal terms depend on several combinations of the elastic parameters via a set of partial derivatives proportional to the partial derivatives of a transversely isotropic medium with a vertical axis of symmetry. This allows us to retrieve anisotropy as a function of depth in the mantle, from the observed azimuthal variations of Love and Rayleigh wave velocities [see *Montagner and Tanimoto,* 1991]. However, the waveform inversion that we use here does not provide direct observations of the azimuthal variation of surface waves velocities. Instead, it provides a path-averaged model for each individual seismogram. *Lévêque et al.* [1998] describe in detail the procedure needed to retrieve the distribution of heterogeneities and anisotropy at depth from the path-averaged models obtained in the waveform inversion. They show that in a long-period approximation, the 1-D SV velocity models obtained after the waveform fitting depend on the combination of elastic parameters best resolved by Rayleigh waves, which control the velocities of SV waves propagating horizontally at azimuth θ. At each depth the path-averaged SV wave velocity perturbation $\delta\hat{\beta}_v$ can be expressed as

$$\delta\hat{\beta}_v = \delta\beta_v + A_1 \cos 2\theta + A_2 \sin 2\theta, \tag{3}$$

where $\delta\beta_v$ is the isotropic perturbation of the SV velocity, θ is the azimuth, $A_1 = (G_c/2\rho\beta_v)$, and $A_2 =$

$(G_s/2\rho\beta_v)$. G_c and G_s are the linear combination of elastic parameters best resolved by Rayleigh waves as defined by *Montagner and Nataf* [1986].

The inversion is performed using the continuous regionalization algorithm of *Montagner* [1986a] for the parameters $\delta\beta_v$, A_1, and A_2. A smoothed model is obtained by assuming a priori a Gaussian correlation between neighboring points, with a specified scale length L_{corr} and a scale factor $\sigma(r)$. This can be represented via an a priori covariance function with the form

$$C_{p0}(r, r') = \sigma(r)\sigma(r') \exp\left[\frac{-\Delta^2_{rr'}}{2L^2_{\text{corr}}}\right], \qquad (4)$$

where $\Delta^2_{rr'}$ is the distance between two geographic points r and r'. The a priori standard deviation $\sigma(r)$ controls the amplitude of the perturbation allowed in the inversion, while the horizontal correlation length L_{corr} acts as a spatial filter that constrains the lateral smoothness of the model. We choose a standard deviation of 0.05 km/s for β_v and 0.003 km/s for A_1 and A_2. The choice of an appropriate correlation length depends on the path coverage and on the period range of inversion. *Montagner* [1986a] suggests the choice of a value of L_{corr} larger than the wavelength and such that the "effective" section of the paths with width L_{corr} ensures a good coverage of the area under study. The anisotropic terms A_1 and A_2 have a variation in 2θ which can be resolved if each cell of width L_{corr} is sampled by at least three paths with different azimuth. After several trials we retained the correlation length of 200 km for β_v, A_1, and A_2 used by *Debayle* [1999]. With the excellent distribution of paths from central Australia to the Tonga-Kermadec trench (Figure 8), a 200 km correlation length is a compromise that favors a smoothed model but should also minimize contamination by diffraction effects. In western Australia, where the distribution of paths is poorer, we have to be more cautious in our discussion of lateral heterogeneities and azimuthal anisotropy.

The continuous regionalization algorithm provides an a posteriori error estimate for the extracted model, which is a very useful guide to the resolution attainable from the data. We have excluded those regions from consideration where the a posteriori error equals the a priori error and these are masked in the figures.

4.2. Results

We have undertaken inversions both with and without azimuthal anisotropy. The lateral variations in SV velocity for an isotropic inversion are represented at six different depths, from 100 to 350 km in Plate 1. The equivalent results for the inversion with azimuthal anisotropy are shown in Plate 2 with the superimposition of a representation of the azimuthal anisotropy pattern at each depth. As can be seen from a comparison of Plates 1 and 2, the pattern of heterogeneity is, in general, not significantly altered by the extraction of the azimuthal anisotropy component. The main difference is an increase in the amplitude of the heterogeneity in the isotropic inversion by 1.9% at a depth of 100 km, reducing to 0.7% at 250 km depth. The largest changes occur in those parts of the model where path coverage is weakest, e.g., in the west.

A posteriori error maps for lateral variations in SV velocity obtained after the inversion including azimuthal anisotropy are presented in Plate 3. The dark blue area on the edge of the maps indicate an a posteriori error close to the a priori error, which can be associated with a total lack of resolution. Ligther blues correspond to regions with smaller a posteriori error, where significant resolution becomes available. These include the whole continent down to 350 km depth with an improved resolution for the region extending from central Australia to the Tonga-Kermadec trench. Note that the a poteriori error reflects the density of crossing paths but also the sensitivity of our fundamental and higher mode dataset to the structure at a given depth. On Plate 3 no significant deterioration of the a posteriori error is observed from 200 to 350 km, indicating that our higher mode data set provides homogeneous resolution in this depth interval.

Cross sections through the SV velocity model (including azimuthal anisotropy) are shown at eight different latitudes from 5°S to 40°S on Plate 4 in a plot which starts at 75 km depth. At depths shallower than 75 km, the results may possibly be affected by the crustal structure that is kept fixed in the inversion. We performed careful crustal corrections based on the 3SMAC model which provides a consistent parametrization of shallow structure across the entire region. Recent interpretation of SKIPPY data using receiver functions [*Shibutani et al.*, 1996; *Clitheroe et al.*, 2000] have revealed a few regions where there are some departures from the crustal model provided by 3SMAC but in general, 3SMAC provides a very good representation of the crust for both the continental and oceanic areas and in addition for the subuction zones. The receiver function models provide point information only for the continent, which is not easily interpolated, and also include the possibility of a gradient zone at the crust-mantle boundary, whereas 3SMAC includes a simple discontinuity and this complicates comparisons. Differences in crustal thickness locally reach 10 km in western Australia beneath the Pilbara craton, in central Australia beneath the Amadeus Basin and in central Queensland. The averaged crustal structure along the path is employed in the inversion and the discrepancies will, in general, affect only a small fraction of a path. However, for the shorter paths the influence of the crustal model may be sufficient to affect the fundamental Rayleigh wave mode at 40 s period and to impose structure in the upper most mantle. As a consequence, we do not display or discuss the shallowest part of the model between the base of the crust and 75 km depth.

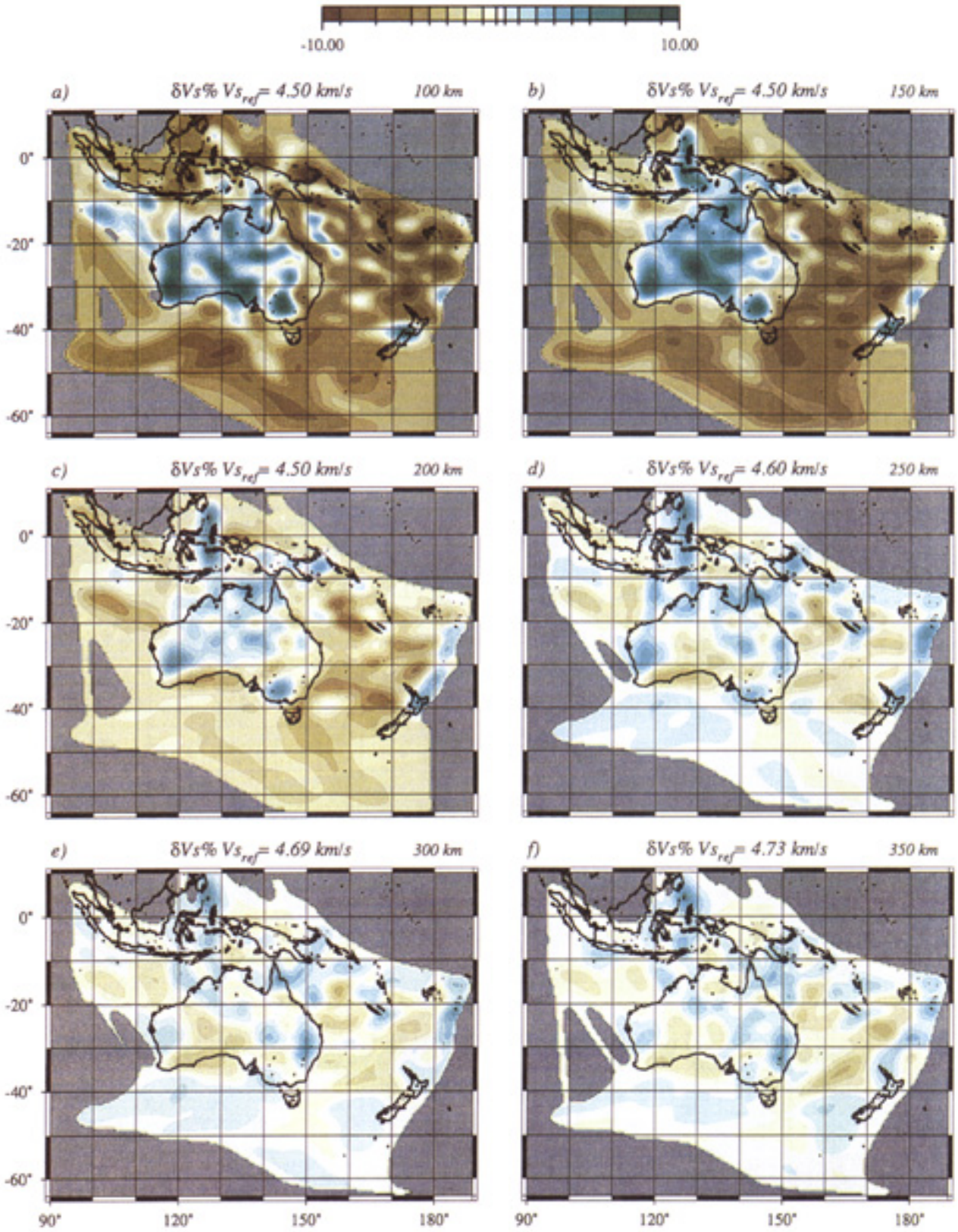

Plate 1. *SV* velocity distribution at different depths from an inversion for just isotropic structure: (a) 100 km, (b) 150 km, (c) 200 km, (d) 250 km, (e) 300 km, and (f) 350 km. The perturbations from the reference velocity at each depth in percent are displayed by color coding. The area in gray on the border of each map corresponds to those regions where the a posteriori error is close to the a priori error, indicating a lack of resolution.

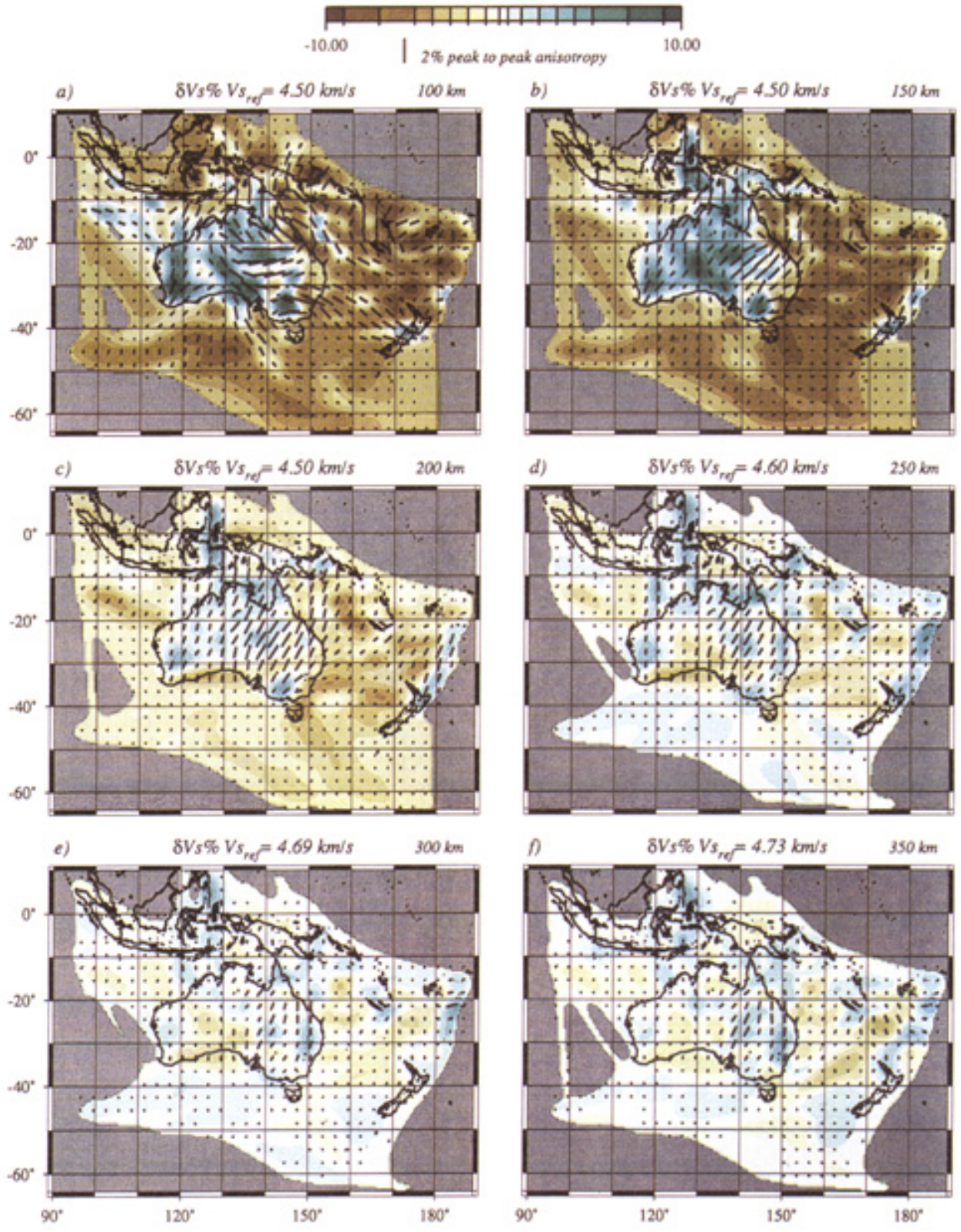

Plate 2. SV velocity distribution from an inversion including azimuthal anisotropy. Fast directions of horizontally propagating SV waves are represented by arrows and superimposed on the SV heterogeneities.

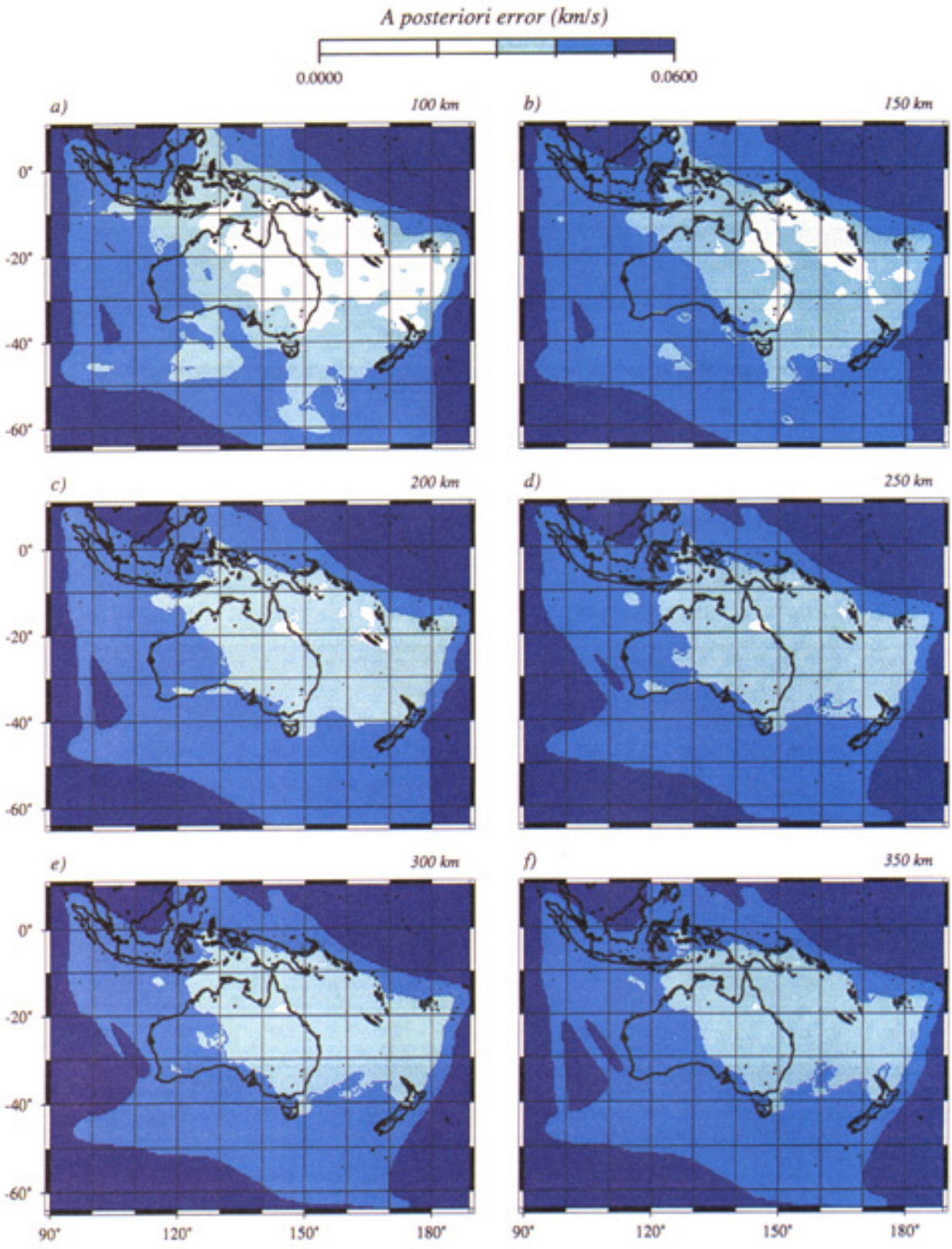

Plate 3. A posteriori error distribution at different depths from the inversion for 3-D structure including azimuthal anisotropy: (a) 100 km, (b) 150 km, (c) 200 km, (d) 250 km, (e) 300 km, and (f) 350 km.

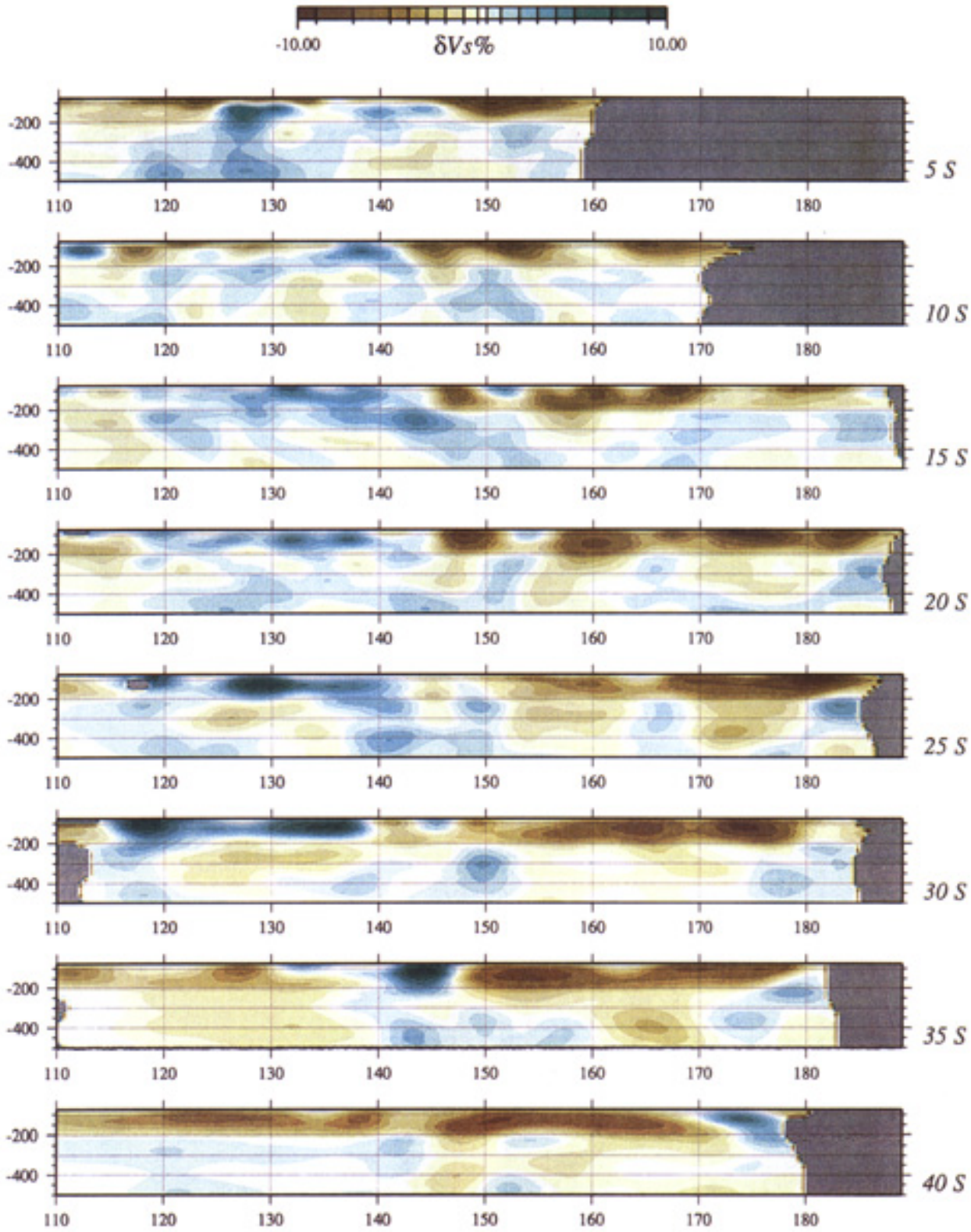

Plate 4. Vertical cross sections through the SV velocity model of Plate 2 at different latitudes (indicated on the right). The cross sections start at 75 km depth and therefore exclude the uppermost mantle, including the oceanic lithosphere. The SV perturbations are indicated with a color scale in percent relative to a common reference model, derived from the average of the SV velocity at each depth. The areas in gray correspond to those regions where the a posteriori error is close to the a priori error indicating a lack of resolution.

4.2.1. Seismic heterogeneity. The heterogeneity patterns in Plates 1 and 2 show a general agreement with the previous results of *Zielhuis and van der Hilst* [1996] and *van der Hilst et al* [1998] for the large-scale features. There is a clear correlation between the main variations in seismic wave speed in the uppermost 200 km of the mantle and surface tectonics. The contrast in seismic wave speed between the eastern Phanerozoic margin of the continent and the central and western Precambrian cratons is confirmed. At 100 km depth (Plate 1a), three regions with high velocities can be recognized within the Precambrian cratons. In western Australia we resolve the average structure along the dominant N-S to NE-SW paths and find high seismic velocities beneath the Archæan Pilbara and Yilgarn cratons. In South Australia, the Archæan Gawler craton is associated with a positive anomaly extending to the northwest beneath the Musgrave Block. This structure vanishes to the north where the north Australian craton extends, from the Kimberley block in Western Australia to the east of Mount Isa. The transition between the Precambrian cratons and the eastern Phanerozoic margin is complex, and south of 25°S, a circular positive anomaly appears east of the Broken Hill Block, extending toward the Lachlan Fold Belt. These features are also retrieved at 150 km depth (Plate 1b) but with a smoother pattern of heterogeneities. In Australia the amplitude of the high-velocity anomaly beneath the Gawler Block is slightly attenuated, but the Lachlan Fold Belt, the Musgrave Block, the Mount Isa Block and the western Archæan cratons remain the four centers of high-velocity anomalies.

At a depth of 200 km the amplitude of seismic contrasts decreases. High velocities remains in northern Australia and around the four centers of high velocities observed at 150 km depth. At 250 km and 300 km depth a broad region of low velocities is present in central Australia, west of 135°E. The high velocities beneath the western Yilgarn and Pilbara cratons are not well constrained in this poorly sampled part of our model and may as well result from horizontal smearing along the dominant paths. On the eastern margin of the continent, where the path coverage is more dense, the New England Fold Belt displays high seismic wave speed below 200 km depth, in agreement with *Zielhuis and van der Hilst* [1996]. However, at shallower depths, no clear high-velocity signature is retrieved in this area.

Finally, a striking feature of Plates 1 and 2 is the set of fast wave speed structures associated with the slabs located on the border of our maps, especially beneath the Philippine, Papua New Guinea, and Tonga Kermadec trenches. These have been isolated because of the good range of crossing paths. Although surface wave inversion does not have the high resolution attainable with delay time analysis, we can follow the slabs on the vertical cross sections (Plate 4) to 500 km depth for the Banda arc at a latitude of 5°S and around 128°E. The Tonga-Kermadec slab can also be followed down to at least 400 km on the cross sections from 20°S to 35°S between 170°E and 190°E. The resolution of the slab anomalies gives us confidence in the potential of our technique to retrieve short-wavelength heterogeneities down to depths as large as 400 km.

4.2.2. Azimuthal anisotropy. On Plate 2 the background color scale represents the variation in seismic wavespeed (as in Plate 1), but azimuthal anisotropy is now represented with bars showing the directions of maximum G computed from the A_1 and A_2 parameters of equation (3). This is the local direction of fast horizontal propagation of SV waves in full, but weak, anisotropy [*Lévêque et al.,* 1998]. The length of the bars is proportional to the percentage of peak to peak azimuthal anisotropy. The amplitude of the azimuthal anisotropy decreases with depth, especially below 200 km, the maximum value of peak to peak azimuthal anisotropy reaching 2.82% at 100 km, 1.90% at 150 km, 1.61% at 200 km, 1.25% at 250 km, 0.87% at 300 km, and 1.01% at 350 km depth. The main change in anisotropic directions occurs between the uppermost 150 km of the model (Plate 2a), where a complex pattern of anisotropy with abrupt changes is observed, and the deeper structure, where azimuthal anisotropy is organized in a much smoother pattern.

At 100 km depth the fast axes appear to have north-south directions beneath the Archæan Pilbara and Yilgarn cratons but may be poorly constrained by the current path coverage in western Australia (Figure 8). The azimuthal coverage is much better farther east and in South Australia, the Archæan Gawler craton and the Musgrave Block display fast directions oriented NW-SE. The north Australian craton reveals a complex anisotropic structure with NE-SW directions beneath the Kimberley Block, changing to NW-SE between the Kimberley and Mount Isa Blocks, and to a dominant east-west direction on the southern margin of the craton near the Arunta Block. South of 20°S, the eastern margin of the continent is dominated by east-west directions. Anisotropy is strong beneath southeast Australia with a dominant east-west component in agreement with the results of *Girardin and Farra,* [1998] for Canberra station (CAN). In the Pacific Ocean the NW-SE directions observed in the Tasman Sea south of 35°S may be biased by the limited azimuthal distribution of paths in this area. North of 20°S, eastern Australia is characterized by NW-SE directions extending in the Coral Sea and turning north-south at the proximity of the New Hebrides trench. A complex, weak anisotropy characterizes the Fiji region.

At 150 km depth the pattern of anisotropy becomes simpler. In central Australia the fast propagation directions are organized with a dominant north-south trend, while farther east, the orientations of the fast directions seems to follow the edge of the Precambrian craton with NE-SW directions on the southeast of Mount

Isa and NW-SE directions on the northeast. We note that anisotropy is stronger on the eastern margin of the continent, compared to central and western Australia. East-west directions are still present beneath southeast Australia but anisotropy vanishes beneath the Tasman Sea. The Coral Sea is associated with north-south directions.

At 200 km depth a smoother pattern of anisotropy is observed. The dominant north-south direction beneath most of Australia turns to NE-SW beneath Mount Isa. This pattern is retrieved at 250 km with a smaller amplitude, and finally, below 250 km depth, anisotropy has almost disappeared everywhere, except in South Australia and Queensland, where a small north-south component remains.

4.3. Testing the Model

To get a better idea of the reliability of the structures appearing in our model, we have performed a number of different types of tests. We first try a synthetic experiment to retrieve the distribution of S wave velocity at a depth of 50 km by the 3SMAC model of *Nataf and Ricard* [1996]. The synthetics are computed for each path in the 3SMAC model and the inversion is performed using the same a priori constraints as in the real case, allowing anisotropy to be present in the model. The input model (Plate 5) presents reasonable features: A sharp increase in velocity is located on the Australian continent around 140°E, at the assumed transition between the eastern Phanerozoic and the central Proterozoic provinces in the 3SMAC model; farther west, another transition occurs near 125°E, representing the assumed boundary between Proterozoic and Archæan cratons. Short-wavelength anomalies are also present in the input model, at -17°S and 137°E in a region well sampled by our paths and at -22°S and 118°E where the density of paths is much weaker. The result is a smoothed image of 3SMAC (Plate 5), but lateral heterogeneities are well retrieved east of 125°E with both the short-wavelength anomaly and the sharp contrast in seismic velocity present in the inverted model. West of 125°E, recovery of the model is not as good because the path coverage is sparser. A slight tendency to smear the anomalies is observed, and the positive anomaly associated with the Archæan craton is shifted toward the Perth region, where few crossing paths are available. Anisotropy is displayed with red bars and is entirely due to the trade-off between the isotropic and the anisotropic part of the model, since no anisotropy is present in the input model. Anisotropy remains very weak everywhere on the map, except near the short-wavelength anomaly in central Australia, where a maximum of 0.5% is observed.

Several other tests have been performed by *Debayle* [1999], and very similar conclusions are obtained with this new data set. We tried to allow short-wavelength heterogeneities by decreasing L_{corr} to 100 km for the SV wave speed. With this value of L_{corr} the level of anisotropy does not decrease and the fast SV directions are unchanged.

We conclude that a small amount of anisotropy is likely to occur in the uppermost 200-250 km of the mantle. In this depth interval, anisotropy can be removed only by accepting a substantial increase in the amplitude of seismic heterogeneities together with a reduction in the level of data fit. In addition, a model with a small amount of anisotropy looks to be in better agreement with other surface waves investigation beneath Australia [e.g., *Gaherty and Jordan,* 1995; *Tong et al.,* 1994]. Below 250 km, the presence of systematic anisotropy is more difficult to demonstrate. The amplitude of observed anisotropy decreases, and imposing an isotropic model does not result in a significant increase in the amplitude of SV perturbations.

For the uppermost 250 km of the model, our dense data set and the synthetic tests suggest that some trade-off between anisotropy and seismic wave speed variations may be present in our maps but is likely to remain small compared with the observed anisotropy. In addition, the observed pattern of anisotropic directions is stable with respect to changes in the degree of smoothing imposed on our model. For example, the drastic changes in anisotropic directions observed at 100 km depth are still present when using a correlation length of 500 km for the anisotropic part of the model, an extreme degree of smoothing with our path coverage. We also note that an error of the order of 20°in the observed anisotropic directions would not change the main features of our model (i.e., the abrupt change in anisotropic directions at shallow depths and the smoother pattern at 150 km depth and deeper). We conclude that even if small biases affect our results, the main features of our maps that are discussed in section 5 are robust.

5. Discussion and Conclusions

5.1. Wave Speed Variation

Our tomographic model shows agreement with previous results obtained for the same region on large scales. For example, the existence of low velocities beneath the eastern margin of Australia compared to the central and western cratons, a feature of the mantle initially revealed by *Cleary et al.* [1972], has been confirmed by regional travel time inversion in southern Australia [*Sambridge,* 1990] and more recent surface waves studies, either global [e.g., *Montagner and Tanimoto,* 1991; *Trampert and Woodhouse,* 1996] or regional and based on the analysis of the Skippy data [*Zielhuis and van der Hilst,* 1996; *van der Hilst et al.,* 1998; *Passier et al.,* 1997]. Our model presents a lateral resolution similar to the one achieved by *van der Hilst et al.* [1998] but is constrained by a larger and more homogeneous data set.

In Western Australia we benefit from the data recorded by the new IRIS station on Cocos island which provides useful east-west crossing paths to those recorded at NWAO and from the data recorded in the Kimba experiment. The improvement is apparent on the velocity maps, which display less smearing on the western margin of the continent. The automated process has allowed us to include a large amount of data from the permanent IRIS and Geoscope stations, providing an excellent distribution of paths in the Pacific Ocean. In this region *Pillet et al.* [1999] obtained phase velocity maps at periods between 8 and 100 s with a lateral resolution not better than 500 km. At depths shallower than 200 km, our more detailed results do not display major discrepancies with the phase velocity maps of *Pillet et al.* [1999] at periods $\geq$ 60 s. There is an agreement at long wavelengths for a low velocity region spanning the North and South Fiji basins. Trenches generally display higher seismic velocities. However, differences occur and in the Coral see, near 152 °E, the corridor of high seismic velocities present in our model is not retrieved by *Pillet et al.* [1999].

A striking feature of Plate 2a is the fact that at 100 km depth the high-velocity anomalies roughly underline the North, South and West cratons as defined by *Myers et al.* [1996] or, in a very similar way, by *Shaw et al.* [1995] on the basis of gravity and magnetic data. Differences occur, for example, at the eastern boundary of the North Australian craton, but the main crustal elements seems to be underlined by a distinct lithospheric signature. An interesting feature is the fast wave speed anomaly, which extends down to 200 km depth beneath the western margin of the Amadeus Basin and Musgrave Block (-25°S, 128°E). To the south, the boundary between the South Australian craton and the Phanerozoic provinces would be close to 140°E. The transition seems, however, complex with an anomalous region of high velocities beneath the Lachlan Fold Belt and the Murray Basin, east of the Broken Hill Block. The model of *van der Hilst et al.* [1998] indicates the presence of a high wave speed in this region, but there is a noticeable difference in the configuration of the wave speed variation. In our results this circular positive anomaly extends deep into the mantle, down to at least 200 km depth, in a region where the crustal thickness provided by the 3SMAC model is close to the one inferred from receiver analysis [*Clitheroe et al.,* 2000]. It is therefore unlikely that the influence of crustal structure is responsible for the anomaly. In addition, the existence of this circular positive anomaly agree well with the 1-D velocity model derived from interstation dispersion measurements in southeastern Australia made by *Passier et al.* [1997]. They found a positive perturbation in S wave velocity between stations SB07 and SB06, both located on our positive anomaly. The negative perturbation that they found between stations SB09 and ZB12 is located in the low-velocity layer of our model, on the northeast of the circular anomaly. The only small difference occurs near the southern coast of Australia, where *Passier et al.* [1997] found a slightly negative perturbation between stations YB07 and YB03, while the perturbation is still slightly positive in our model. Slight smearing of the anomaly toward the south where the path coverage is less dense in our model may explain this small difference. We also note that the edge of this circular feature is clearly outlined by the gravity and magnetic data [*Murray et al.,* 1997; *Tarlowski et al.,* 1996; see also *Wellman,* 1998], which suggests that what we see here is mantle structure linked to crustal features. The entire area is blanketed with thick sediment so there is no basement exposure available.

Vertical cross sections in our model (Plate 4) cross the Australian continent from 15°S to 35°S, suggesting significant variations in the lid thickness. Such variations have been observed in previous tomographic studies of Australia, and *van der Hilst et al.* [1998] argue for a lithosphere thickness that would reach at least 350 km in some parts of the continent. On Plate 4, a lid that is between 200 and 300 km thick may be present in the extreme north of the continent at a latitude of 15°S, with a deeper structure east of 140°E. However, south of 20°S, a low-velocity zone is observed below around 200 km for most of the Australian mantle. In addition, beneath Australia we observe locally high-velocity anomalies extending from the surface to 500 km depth (e.g., around 140°E on the vertical cross section at -25°S). This kind of structure may well result from the superposition of two distinct relatively thick positive anomalies separated by a thin low-velocity layer that cannot be resolved with the Rayleigh wave data with periods of at least 40 s used in this study. In the case of the thick positive anomaly at 25°S this hypothesis is supported by the observation that at 20°S and 30°S, shallow and deep positive anomalies are separated by a low-velocity layer located between around 200 and 300 km. This kind of artefact may be frequent in surface wave inversion for mantle structure where the current period range of analysis makes it difficult to resolve vertical structures with dimensions $<$ 100 km. The existence of a slight low-velocity zone for SV velocity at around 200 km for most of the Precambrian mantle beneath Australia is supported by the path-averaged velocity models in Figure 7 (paths 1, 2, 3, 4, 7, 8, 10, and 11). The average model for northern Australia built by *Kennett et al.* [1994] from body waves analysis has a low-velocity layer associated with low Q [*Gudmundsson et al.,* 1994] below 210 km. The widespread presence of such a feature beneath the cratonic regions is supported by the body wave analysis of *Kaiho and Kennett,* [2000] using the Skippy and Kimba data. We note also the good agreement between the S wave model of *Kennett et al.* [1994] and our shear velocity structure for path 1, which samples the northern part of Australia (Figure 7, model 1). The slightly thicker lid observed on the section at 15°S (Plate 4) may reflect the differences between the local structure beneath the path and the

average model for northern Australia obtained by *Kennett et al.* [1994].

The base of the high-velocity lid remains difficult to define accurately from seismic anomalies. From the path averaged models of Figure 7 and using the strongest negative gradient as indicator, we would place the base of the lid somewhere between 150 and around 200 km for most of Precambrian Australia. However, the cross sections in the tomographic model (Plate 4) and the map at 200 km in Plate 2c suggest that for a significant part of the continent, the thickness of the high-velocity lid reaches or exceeds 200 km. A slight low-velocity layer is probably present just below the lid. The existence of deep anomalies below 400 km with apparent connections to the surface is locally observed but may result from the superposition of distinct positive anomalies. South of Mount Isa (at around 140°E and 25 °S), however, the vanishing of the low-velocity layer is likely to be associated with an anomalous thick lid that may reach 300 km, as suggested in previous studies.

The main differences from the model presented by *van der Hilst et al.* [1998] and more recently by *Simons et al.* [1999] occur below 200 km and so may be related to the treatment of higher mode information and the way in which the averaged models are interpreted. In the CL approach to waveform inversion the fundamental and higher modes are treated together, and the highest frequency that we have used is 0.025 Hz (40 s period). In contrast, the PWI approach used by *Zielhuis and van der Hilst,* [1996] and *van der Hilst et al.,* [1998] separates the fundamental and higher mode segments of the seismograms by group velocity filtering and then uses different frequency bands for the inversion of the segments. Frequencies up to 0.05 Hz have been considered for the higher modes, which approach the limits of the simple approximations underlying the technique. The size of wave speed variations across the region suggests that mode coupling may need to be taken into consideration for the higher modes at short periods. Since both styles of inversion are expected to have similar nominal resolution, the differences suggest that we should be wary of interpreting features on scales < 300 km in these models.

5.2. Anisotropy

The comparison of our azimuthal anisotropy maps with other results is not straightforward, since no previous surface waves work is available with a comparable lateral resolution, except the results of the preliminary inversion reported by *Debayle* [1999]. As observed by *Debayle* [1999], a complex pattern of anisotropy is observed at shallow depths, turning to a smoother pattern at a depth of 150 km. This is supported by recent global azimuthal anisotropy maps (*J. Trampert, personal communication*, 1999), and in a general way, the smooth anisotropy obtained at depths larger than 150 km agree with previous global [e.g., *Montagner and Tanimoto,* 1991] and regional [*Lévêque et al.,* 1998] studies. Some *SKS* observations are available for the Precambrian cratons of Australia [*Clitheroe and van der Hilst,* 1998], but most of the splitting has been attributed to the crust. On the eastern margin of the continent, where a deeper origin is plausible, the observed directions may result from the superposition of two anisotropic layers with different fast axis azimuth [*Girardin and Farra,* 1998]. At the permanent CAN station our results are in qualitative agreement with the two layered anisotropic model of *Girardin and Farra* [1998]. Our directions are also consistent with *SKS* splitting observations at the NWAO and CTAO stations [*Vinnik et al.,* 1992]. The general agreement with previous work allows us to be confident in a more detailed analysis of our maps.

The most striking feature of Plate 2 is a drastic change from a complex anisotropy in the uppermost 150 km of the model to a smoother pattern at larger depth with an alignment of fast axis close to the current direction of plate motion. This suggests an association of the shallow anisotropy with past deformations "frozen" in the lithosphere, while the deeper part would correspond to present deformation due to the northward motion of the Australian plate.

Our understanding of the relationship between crystallographic orientation and mantle deformation comes from theoretical studies and observations of mantle peridotites [*Nicolas and Poirier,* 1976; *McKenzie,* 1979; *Christensen,* 1984; *Nicolas and Christensen,* 1987; *Ribe and Yu,* 1991; *Mainprice and Silver,* 1993]. In a general way, the fast a axis of olivine crystals is expected to be parallel to the direction of maximum extension. However, for large strain and at sufficiently high temperature and pressure (1500 K and 300 MPa), simple shear should orient the a axis closer to the flow direction [*Zhang and Karato,* 1995]. At the bottom of the plate we expect the relative movement of the lithosphere over the underlying mantle to produce simple shear. Whether anisotropy is parallel to the flow or closer to the maximum extension direction is not critical as we only resolve the horizontal projection of seismic anisotropy, which in both cases is along the azimuth of the flow. At lithospheric depths we expect the a axis of olivine crystals to be close to the extension direction. In a collisional regime the extension direction is in the plane perpendicular to the collision direction and can be either vertical or horizontal. For a vertical a axis we would expect no significant azimuthal anisotropy, and for departure from the vertical, azimuthal anisotropy should orient with the axis of greatest horizontal elongation, perpendicular to the collision directions. For strike-slip boundaries, azimuthal anisotropy is expected to be in the extension direction, close to the azimuth of the fault for large strains. The relations between observed azimuthal anisotropy and the tectonic processes responsible for mantle deformation are therefore very similar to those discussed by *Silver and Chan* [1991] for vertically travelling core shear phases.

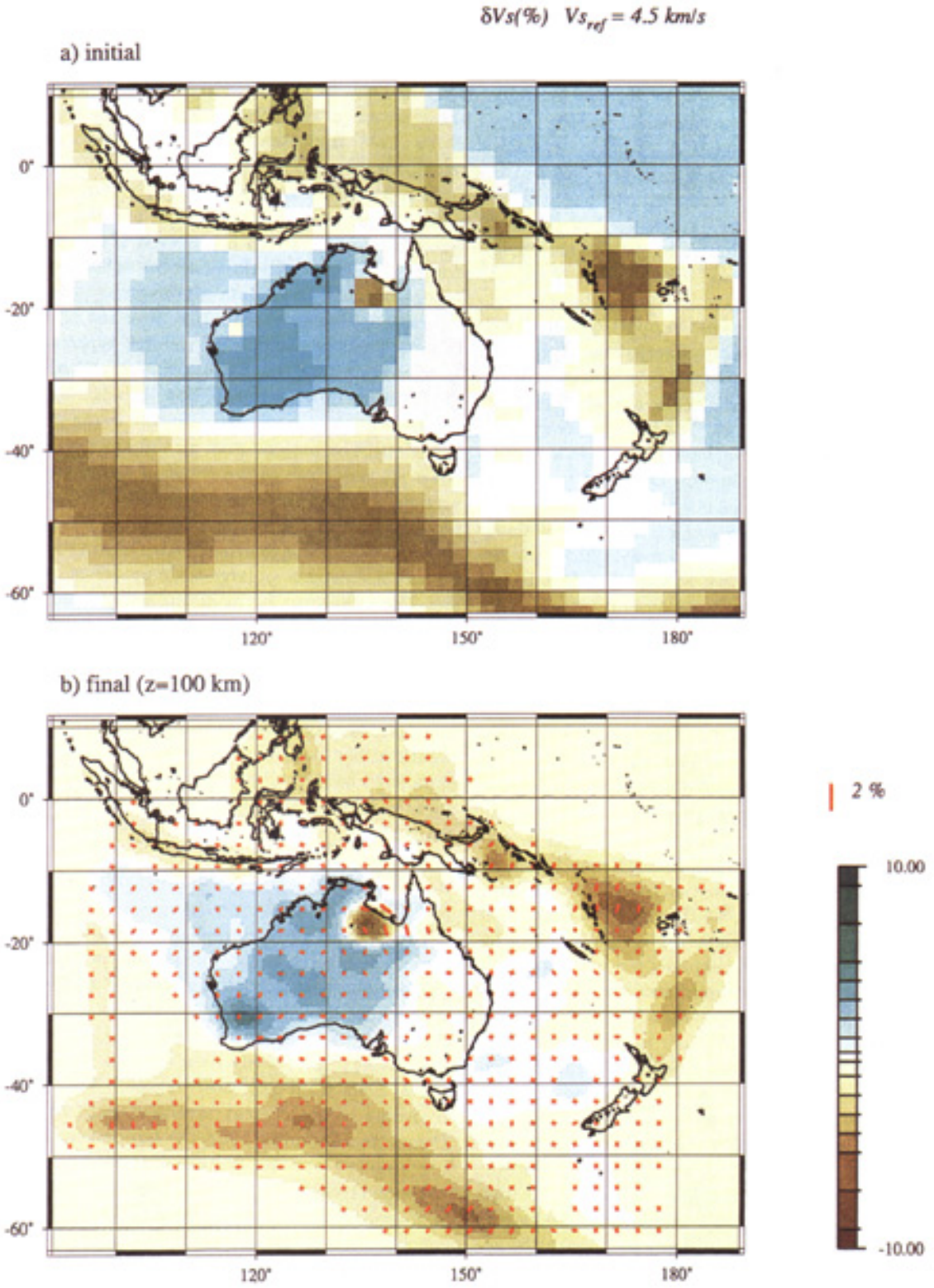

Plate 5. Synthetic experiment on the trade-off between velocity and anisotropy. (a) The input model for the shear wave velocity at a depth of 50 km for the isotropic 3SMAC model of *Nataf and Ricard* [1996]. (b) The azimuthal anisotropy arising from the trade-off between heterogeneity and azimuthal anisotropy

Since Archæan times, a large number of tectonic events affected the diverse components of Australia. Most of the important faults have acted in compression, extension, or strike slip many times, and in theory, it would probably be possible to find a tectonic event that explains any pattern of anisotropy in many parts of Australia. Our investigation is, however, simplified by the fact that the mobility of olivine crystals at temperatures below 1100-1200 K is very low but is sharply enhanced at higher temperatures [e.g., *Estey and Douglas,* 1986]. Thus we expect the last thermal event that heated the lithosphere above the threshold value to erase old anisotropy and to control the observed pattern.

The main evidence that would support the presence of frozen anisotropy in the lithosphere comes from the east-west trend observed at 100 km depth in central Australia beneath the Arunta Block and the north of the Amadeus Basin (Plate 2a). The last significant tectonic event that affected central Australia is a north-south compression during the late Devonian to middle Carboniferous (350-320 Ma) Alice Springs orogeny. The main lithospheric shortening was accommodated along the Redbank Thrust Zone, an east-west lithospheric scale shear zone located north of the Amadeus Basin and extending to depth of at least 50 km [*Shaw et al.,* 1992]. The east-west direction of fast SV wave propagation in central Australia at depths shallower than 150 km follows closely the Redbank Thrust Zone located at a latitude close to 24°S and eastward of 130°E. More generally, the east-west fast directions observed in central Australia would be in agreement with a north-south compression between two rigid blocks, the North Australian and the South Australian cratons [*Shaw et al.,* 1996].

Frozen anisotropy in the lithosphere would also be supported by the observation that the three Precambrian crustal blocks (North, South, and West Australian cratons) have a distinct anisotropic signature. The West Australian craton has experienced a north-south to NE-SW extension contemporaneous with the Alice Springs orogeny. This is in general agreement with our anisotropic directions, but the poor azimuthal coverage available in western Australia makes further discussion futile. The NE-SW anisotropy beneath the Kimberley follows the geological trend [*Wellman,* 1998], but it is less clear for some other parts of the North Australian craton. We would for example expect north-south directions beneath the Mount Isa and Georgetown Inliers [*Wellman,* 1998]. In South Australia, the NW-SE anisotropy is also in disagreement with the geological trends on the western part of the Gawler craton. Anisotropy on the eastern margin of the continent has a complex pattern and seems to follow the edge of the North Australian craton north of 25°S. Alternatively, the east-west direction on the southern margin of the North Australian craton may be related to the lateral extrusion of material following the north-south compression during the Alice Springs orogeny [*J. Braun, personal communication,* 1999]. South of 25°S, the roughly east-west directions are more difficult to explain as they do not fit with a simple model of terrane accretion on the margin of a craton. However, our directions beneath Canberra are in good agreement with those obtained at lithospheric depth by *Girardin and Farra* [1998] from analysis of shear wave splitting for teleseisms.

As reported by *Debayle* [1999], the depth of 150 km represents an abrupt change in the anisotropy distribution. A smooth pattern is observed (Plate 2b), with a dominant north-south direction in central and western Australia. The large data set involved in the current inversion allows us to refine the direction of anisotropy in some parts of the map at 150 km, especially on the eastern margin of the continent, east of 140°E, where the fast directions seem to follow the edge of the craton (Plate 2b), a less pronounced feature in the preliminary inversion. The present map at 150 km depth remains, however, very close to the result of the preliminary inversion, yielding the same conclusion: The smooth pattern observed at 150 km depth is clearly not compatible with short-wavelength lithospheric deformations and requires the existence of large-scale processes in the mantle. The agreement between our anisotropic directions in central and western Australia and the northward movement of the Australian plate suggests the most likely candidate is shearing of the mantle by the plate motion. Shearing compatible with present-day deformation is thus observed in the Australian Precambrian mantle at depths as shallow as 150 km (Plate 2b). This apparent change in the nature of seismic anisotropy does, however, not seem to be associated with a clear change in the S velocity structure even though a change in anisotropy has often been associated with a change in seismic velocities [e.g., *Karato,* 1992; *Gaherty and Jordan,* 1995].

The wave speed variations as displayed in Plates 1, 2, and 4 show no noticeable change in character near 150 km depth where the anisotropy changes. It would appear that present-day deformation is occuring within the region of high seismic wave speeds. Similar conclusions have previously been reached by Vinnik et al. [1992, 1995] from *SKS* observations. They noted that according to the current accepted geotherm [see, e.g., *Davies and Richards,* 1992] the temperature within the Precambrian cratons is likely to reach the threshold value of 1100-1200 K, at which the mobility of olivine is sharply enhanced just above 150 km depth. They conclude that below 150 km depth, past deformation is not likely to be preserved as it would be erased by more recent deformation. Our results support this scenario.

The high seismic wave speeds outlining the "lid" would correspond to a "seismic" definition of the lithosphere likely to be related to processes in the mantle of thermal or compositional origin (e.g., via depletion of the cratonic keel). The depth at which present-day

deformation occurs within the upper mantle would define a "mechanical" lithosphere, the part of the mantle which has coherent horizontal motion. Present deformation in the base of the high-velocity lid may thus occur when the conditions in the mantle at a given depth favor the orientation of olivine crystals. This in turn implies a correlation between the lid thickness and the depth at which present-day deformation is observed. We note that in the thickest part of the root, where the mantle is cooler, a larger resistance to mantle flow is opposed. This can be seen near Mount Isa and the Lachlan Fold Belt, where a NE-SW deflection of the anisotropy is observed between 150 and 200 km depth (Plate 2b, c). The tentative observation that the deep positive anomaly beneath Mount Isa and the Lachlan Fold Belt are progressively shifted toward the south from 200 to 300 km suggests that significant shearing occurs, deforming the deep part of the root by a few hundred kilometers in few hundred million years. Finally, east of 140°E, the anisotropy directions are not simply related to the northern motion of the Australian plate at 150 km depth. A possible scenario is to invoke channelling of the asthenospheric flow around the edge of the craton to explain the NE-SW directions east of 140°E. A similar model has already been proposed for central Europe [*Bormann et al.,* 1996] and is plausible in North America [*Barruol et al.,* 1997; *Fouch et al.,* 1997].

Present-day deformation appears to occur between 150 and 250 km depth beneath Precambrian Australia. The upper limit seems to be related to the mobility of olivine crystals in the Precambrian mantle. The lower limit may be associated with the vanishing of significant deformation or with a change in the mode of deformation, e.g., from dislocation creep to diffusion creep, as suggested by *Karato* [1992]. Below 250 km we found no clear evidence of azimuthal anisotropy. Our observations are thus complementary to the results of *Gaherty and Jordan* [1995], who found significant anisotropy located in the upper 250 km of the mantle in a transversely isotropic model for a single NW-SE corridor across Australia. It seems, however, that the azimuthal anisotropy cannot be simply interpreted as frozen in the lithosphere, since plate motion deformation is inferred in the mantle below 150 km depth. This agrees with the results of *Tong et al.* [1994], and *Lévêque et al.* [1998] and with the previous study of *Girardin and Farra* [1998] for eastern Australia.

Finally, we note that our results for Precambrian Australia are consistent with models for other shield regions. A slight low-velocity layer for S waves at a depth of around 200 km has been found beneath the Canadian Shield [*Brune and Dorman,* 1963], the Baltic Shield [*Calcagnile,* 1991], and southern Africa [*Qiu et al.,* 1996]. In southern Africa the average lithospheric structure has been determined from teleseismic receiver functions, travel time measurements, and waveform inversion of surface waves. *Qiu et al.* [1996] proposed a high-velocity lid 120 km thick underlain by a low-velocity zone. However, a revised S wave model has been suggested for the same region that satisfies both regional seismic waveform data and the fundamental mode Rayleigh wave phase velocity data for the region [*Priestley,* 1999]. This model includes a high-velocity lid that extends to 160 km for the Archæan core. In addition, anisotropy parallel to the flow was found beneath the Kaapvaal craton of southern Africa by *Vinnik et al.* [1995]. They conclude that present-day deformation should occur below 150 km in the mantle and perhaps until 400 km depth. Our results would support their suggestion that the deep continental root defined by the seismic anomalies may be deformed by plate motion.

The observation that at least two layers with significant anisotropy but different directions are observed in the Australian continental mantle suggests that care should be taken in the interpretation of anisotropy directions from observations of *SKS* splitting. There is a critical need to develop techniques for mapping anisotropy as a function of depth. Work is in progress for the Australian region on the polarization anisotropy inferred from the discrepancy in dispersion between Love and Rayleigh waves as a means of investigating the depth extent of anisotropy using an independent data set.

Appendix A: Path-Averaged SV Velocity Models

In this appendix we demonstrate that the averaging of phase slowness along the path implies that the 1-D model recovered from the waveform inversion will represent an average of the shear slowness along the path.

Equation (1) can be applied to perturbations in phase slowness and becomes

$$\Delta\left[\frac{1}{C_i^{\mathrm{es}}}\right] = \frac{1}{L^{\mathrm{es}}}\int_{\mathrm{es}} \Delta\left[\frac{1}{C_i^{\mathrm{loc}}}\right] ds, \qquad \text{(A1)}$$

where the index i denotes period.

The relation between a perturbation of the phase slowness $\Delta[1/C_i]$ (for period i) and a perturbation of SV slowness $\Delta[1/\beta_{vj}]$ (at depth j) is weakly nonlinear and can be approximated with the following first-order relation:

$$\Delta\left[\frac{1}{\beta_v}\right]_j = \sum_i H_{ji}\Delta\left[\frac{1}{C}\right]_i, \qquad \text{(A2)}$$

where H_{ji} is the operator which contains the partial derivatives of the phase slowness with respect to shear slowness which can be found from the results given by, e.g., *Takeuchi and Saito* [1972]. Substituting (A1) in (A2) yields

$$\Delta\left[\frac{1}{\beta_v^{\mathrm{es}}}\right]_j = \frac{1}{L^{\mathrm{es}}}\int_{\mathrm{es}} \sum_i H_{ji}\Delta\left[\frac{1}{C^{\mathrm{loc}}}\right]_i ds \qquad \text{(A3)}$$

and also from (A2)

$$\Delta\left[\frac{1}{\beta_v^{\mathrm{loc}}}\right]_j = \sum_i H_{ji}\Delta\left[\frac{1}{C^{\mathrm{loc}}}\right]_i, \qquad \text{(A4)}$$

where β_v^{loc} is the local value of the shear velocity at each point (θ, ϕ) along the path at a depth j. We can therefore express the effective shear slowness for the path at depth j as a path integral of the shear slowness in the local models at this depth

$$\frac{1}{\beta_{vj}^{\mathrm{es}}} = \frac{1}{L^{\mathrm{es}}}\int_{\mathrm{es}} \frac{1}{\beta_{vj}^{\mathrm{loc}}}\, ds. \qquad \text{(A5)}$$

Thus the 1-D SV models β_{vj}^{es} obtained from the waveform inversion can be regarded as corresponding to the integral of the local shear slowness along the path.

Acknowledgments. We would like to thank O. Gudmundsson, M. Sambridge, J. Braun, R. Shaw, L. Rivera, and J. J. Lévêque for many helpful discussions at various stage of this work. We are grateful to K. Yoshisawa, who performed ray-tracing experiments in our tomographic model, and we acknowledge J. Trampert for providing a preprint of his anisotropy maps before publication. We also thank the Geoscope team (especially G. Guiveneux and G. Roult) and the IRIS team for providing seismological data at the permanent stations. The management of the data from the portable experiments was made possible by the system established by Rob van der Hilst. Finally, special thanks are addressed to Steven Sirotjuk, Armando Arcidiaco, Tony Percival, John Grant, Darryn Schneider, Paul Johnston, and the RSES personnel who collected the Skippy and Kimba data on the field. The maps and the cross section presented in this paper have been made using the GMT software.

References

Barruol, G., P.G. Silver, and A. Vauchez, Seismic anisotropy in the eastern United States: Deep structure of a complex continental plate, *J. Geophys. Res., 102*, 8329–8348, 1997.

Bormann, P., G. Gruenthal, R. Kind, and H. Montag, Upper mantle anisotropy underneath central Europe: Effect of absolute plate motion and lithosphere-asthenosphere boundary topography?, *J. Geodyn., 22*, 11-32, 1996.

Brune, J., and J. Dorman, Seismic waves and Earth structure in the Canadian Shield, *Bull. Seismol. Soc. Am., , 53*, 167-210, 1963.

Calcagnile, G., Deep structure of Fennoscandia from fundamental and higher mode dispersion of Rayleigh waves, *Tectonophysics, 195*, 139-149, 1991.

Cara, M., Regional variations of higher Rayleigh-mode phase velocities: A spatial-filtering method, *Geophys. J. R. Astron. Soc., 54*, 439-460, 1978.

Cara, M., Lateral variations of S velocity in the upper mantle from higher Rayleigh modes, *Geophys. J. R. Astron. Soc., 57*, 649-670, 1979.

Cara, M., and J.J. Lévêque, Waveform inversion using secondary observables, *Geophys. Res. Lett., 14*, 1046-1049, 1987.

Cara, M., and J.J. Lévêque, Anisotropy of the asthenosphere: The higher mode data of the Pacific revisited, *Geophys. Res. Lett., 15*, 205-208, 1988.

Christensen, N.I., The magnitude, symmetry and origin of upper mantle anisotropy based on fabric analyses of ultramafic tectonics, *Geophys. J. R. Astron. Soc., 76*, 89-112, 1984.

Christensen, N.I., and M.H. Salisbury, Seismic anisotropy in the oceanic upper mantle: Evidence from the Bay Islands Ophiolite Complex, *J. Geophys. Res., 84*, 4601-4610, 1979.

Cleary, J.R., D.W. Simpson, and K.J. Muirhead, Variations in the Australian upper mantle structure from observations of the cannikin explosion, *Nature, 236*, 111-112, 1972.

Clitheroe, G., and R.D. van der Hilst, Complex anisotropy in the Australian lithosphere from shear-wave splitting in broad-band *SKS* records, in *Structure and Evolution of the Australian Continent*, edited by J. Braun et al., Geodyn. Ser., vol. 26, pp. 73-78, AGU, Washington, D.C., 1998.

Clitheroe, G., O. Gudmundsson, and B.L.N. Kennett, The crustal structure of Australia, *J. Geophys. Res., , 105*, 13,697-13,713, 2000.

Davies, G.F., and M.A. Richards, Mantle convection, *J. Geol., 100*, 151-206, 1992.

Debayle, E., Tomographie du manteau supérieur de l'Océan Indien par inversion de forme d'ondes, thèse de doctorat, 156 pp., Univ. Louis Pasteur, Strasbourg, France, 1996.

Debayle, E., SV wave azimuthal anisotropy in the Australian upper-mantle: Preliminary results from automated Rayleigh waveform inversion, *Geophys. J. Int., 137*, 747-754, 1999.

Dziewonski, A.M., Upper mantle models from "pure-path" dispersion data, *J. Geophys. Res., 76*, 2587-2601, 1971.

Dziewonski, A.M., and D.L. Anderson, Preliminary reference Earth model, *Phys. Earth Planet. Inter., 25*, 297-356, 1981.

Estey, L.H., and B.J. Douglas, Upper mantle anisotropy: A preliminary model, *J. Geophys. Res., 91*, 11,393-11,406, 1986.

Fleitout, L., and D.A. Yuen, Secondary convection and the growth of the oceanic lithosphere, *Phys. Earth Planet. Inter., 36*, 181-212, 1984.

Forsyth, D.W., The early structural evolution and anisotropy of the oceanic upper mantle, *Geophys. J. R. Astron. Soc., 43*, 103-162, 1975.

Fouch, M.J., K.M. Fisher, and E.M. Parmentier, Shear wave splitting, continental roots, and patterns of mantle flow, *Eos Trans. AGU, 78*(46), Fall Meet. Suppl., F5, 1997.

Gaherty, J.B., and T.H. Jordan, Lehmann discontinuity as the base of anisotropic layer beneath continents, *Science, 268*, 1468- 1471, 1995.

Gee, L.S., and T.H. Jordan, Generalized seismological data functionals, *Geophys. J. Int., 111*, 363-390, 1992.

Girardin, N., and V. Farra, Azimuthal anisotropy in the upper mantle from observations of P-to-S converted phases: Application to southeast Australia, *Geophys. J. Int., 133*, 615-629, 1998.

Gudmundsson, O., B.L.N. Kennett, and A. Goody, Broadband observations of upper-mantle seismic phases in northern Australia and the attenuation structure in the upper mantle, *Phys. Earth Planet. Inter., 84*, 207-226, 1994.

Jordan, T.H., The continental tectosphere, *Rev. Geophys., 13*(3), 1-12, 1975.

Kaiho, Y., and B.L.N. Kennett, Three-dimensional seismic structure beneath the Australasian region from refracted wave observations *Geophys. J. Int.*, in press, 2000.

Karato, S.I., On the Lehmann discontinuity, *Geophys. Res. Lett., 19*, 2255-2258, 1992.

Kennett, B.L.N., Approximations for surface-wave propagation in laterally varying media, *Geophys. J. Int., 122*, 470-478, 1995.

Kennett, B.L.N., O. Gudmundsson, and C. Tong, The upper-mantle *S* and *P* velocity structure beneath northern Australia from broad-band observations *Phys. Earth Planet. Inter., 86*, 85-98, 1994.

Lerner Lam, A.L., and T.H. Jordan, Earth structure from fundamental and higher modes analysis, *Geophys. J. R. Astron. Soc., 75*, 759-797, 1983.

Lévêque, J.J., Regional upper-mantle S-velocity models from phase velocities of great Rayleigh waves, *Geophys. J. R. Astron. Soc., 63*, 23-43, 1980.

Lévêque, J.J., M. Cara, and D. Rouland, Waveform inversion of surface wave data: Test of a new tool for systematic investigation of upper mantle structures, *Geophys. J. Int., 104*, 565-581, 1991.

Lévêque, J.J., E. Debayle, and V. Maupin, Anisotropy in the Indian Ocean upper mantle from Rayleigh- and Love-waveform inversion, *Geophys. J. Int., 133*, 529-540, 1998.

Li, X.D., and T. Tanimoto, Waveforms of long-period body waves in a slightly aspherical Earth model, *Geophys. J. Int., 112*, 92-102, 1993.

Mainprice, D., and P.G. Silver, Interpretation of *SKS*-waves using samples from the subcontinental lithosphere, *Phys. Earth Planet. Inter., 78*, 257-280, 1993.

Marquering, H., and R. Snieder, Surface-wave mode coupling for efficient forward modelling and inversion of body-wave phases, *Geophys. J. Int., 120*, 186-208, 1995.

Marquering, H., R. Snieder, and G. Nolet, Waveform inversions and the significance of surface-wave mode coupling, *Geophys. J. Int., 124*, 258-278, 1996.

McKenzie, D., Finite deformation during fluid flow, *Geophys. J. R. Astron. Soc., 58*, 689-715, 1979.

Montagner, J.P., Regional three-dimensional structures using long-period surface waves, *Ann. Geophys. 4*, 283-294, 1986a.

Montagner, J.P., 3-dimensional structure of the Indian Ocean inferred from long-period surface waves, *Geophys. Res. Lett., 13*, 315-318, 1986b.

Montagner, J.P., and N. Jobert, Vectorial tomography, 2, Application to the Indian Ocean, *Geophys. J. R. Astron. Soc., 94*, 309-344, 1988.

Montagner, J.P., and H.C. Nataf, A simple method for inverting the azimuthal anisotropy of surface waves, *J. Geophys. Res., 91*, 511-520, 1986.

Montagner, J.P., and T. Tanimoto, Global anisotropy in the upper mantle inferred from the regionalization of phase velocities, *J. Geophys. Res., 95*, 4797-4819, 1990.

Montagner, J.P., and T. Tanimoto, Global upper mantle tomography of seismic velocities and anisotropies, *J. Geophys. Res., 96*, 20,337-20,351, 1991.

Murray, A.S., M.P. Morse, P.R. Milligan, and T.E. Mackey, Gravity anomaly map of the Australian region, 2nd ed., scale 1:5 000 000, Aust. Geol. Surv. Org., Canberra, 1997.

Myers, J.S., R.D. Shaw, and I.M. Tyler, Tectonic evolution of Proterozoic Australia, *Tectonics, 15*, 1431-1446, 1996.

Nataf, H.C., and Y. Ricard, 3SMAC: An a priori tomographic model of the upper mantle based on geophysical modeling, *Phys. Earth Planet. Inter., 95*, 101-122, 1996.

Nataf, H.C., I. Nakanishi, and D.L. Anderson, Anisotropy and shear-velocity heterogeneities in the upper mantle, *Geophys. Res. Lett., 11*, 109-112, 1984.

Nicolas, A., and N.I. Christensen, Formation of anisotropy in upper mantle peridotites–A review, in *Composition, Structure and Dynamics of the Lithosphere-Asthenosphere System, Geodyn. Ser.*, vol. 16, edited by F. Fuchs and C. Froidevaux, pp. 111-123, AGU, Washington, D. C., 1987.

Nicolas, A., and J.P. Poirier, *Crystalline Plasticity and Solid State Flow in Metamorphic Rocks*, 444 pp., John Wiley, New York, 1976.

Nishimura, C.E., and D.W. Forsyth, The anisotropic structure of the upper mantle in the Pacific, *Geophys. J. Int., 96*, 203-229, 1989.

Nolet, G., Higher Rayleigh modes in western Europe, *Geophys. Res. Lett., 2*, 60-62, 1975.

Nolet, G., Partitioned waveform inversion and two dimensional structure under the network of autonomously recording seismographs, *J. Geophys. Res., 95*, 8499-8512, 1990.

Okal, E.A., The effect of intrinsic ocean upper mantle heterogeneity on the regionalization of long period rayleigh wave phase velocities, *Geophys. J. R. Astron. Soc., 49*, 357-370, 1977.

Passier, M.L., R.D. van der Hilst, and R.K. Snieder, Surface wave waveform inversions for local shear-wave velocities under eastern Australia, *Geophys. Res. Lett., 24*, 1291-1294, 1997.

Peselnick, L., and A. Nicolas, Seismic anisotropy in an ophiolite peridotite: Application to oceanic upper mantle, *J. Geophys. Res., 83*, 1227-1235, 1978.

Pillet, R., D. Rouland, G. Roult, and D.A. Wiens, Crust and upper mantle heterogeneities in the southwest Pacific from surface wave phase velocity analysis, *Phys. Earth Planet. Inter., 110*, 211-234, 1999.

Priestley, K., Velocity structure of the continental upper mantle: Evidences from southern Africa, *Lithos, 48*, 45-56, 1999.

Qiu, X., K. Priestley, and D. McKenzie, Average lithospheric structure of southern Africa, *Geophys. J. Int., 127*, 563-587, 1996.

Ribe, N., and Y. Yu, A theory for the evolution of orientation textures in deformed olivine polycrystals, *J. Geophys. Res., 96*, 8325-8335, 1991.

Ricard, Y., H.C. Nataf, and J.P. Montagner, The three-dimensional seismological model a priori constrained: Confrontation with seismic data, *J. Geophys. Res., 101*, 8457-8472, 1996.

Roult, G., D. Rouland, and J.P. Montagner, Velocity distribution in the Indian Ocean and Indonesian region inferred from Geoscope records, *Geophys. Res. Lett., 14*, 343-346, 1987.

Sambridge, M.S., Non-linear arrival time inversion: Constraining velocity anomalies by seeking smooth models in 3-D, *Geophys. J. Int., 102*, 653-677, 1990.

Shaw, R.D., B.R. Goleby, R.J. Korsch, and C. Wright, Basement and cover thrust tectonics in central Australia based on the Arunta-Amadeus seismic reflection profile, in *Basement Tectonics*, edited by M.J. Rickard, H.J. Harrington, and P.R. Williams, pp. 55-84, Kluwer Acad., Norwell, Mass., 1992.

Shaw, R.D., P. Wellman, P. Gunn, A.J. Whitaker, C. Tarlowski, and M. Morse, Australian crustal element map: A geophysical model for the tectonic framework of the continent, *Aust. Geol. Surv. Org. Res. Newsl., 23*, 1-3, 1995.

Shaw, R.D., P. Wellman, P. Gunn, A.J. Whitaker, C. Tarlowski, and M. Morse, Users guide to the Australian crustal element map, *Aust. Geol. Surv. Org. Rec., 1996/30*, 93 pp., 1996.

Shibutani, T., M. Sambridge, and B.L.N. Kennett, Genetic algorithm inversion for receiver functions with application to crust and uppermost mantle structure beneath eastern Australia, *Geophys. Res. Lett., 23*, 1829-1832, 1996.

Silveira, G., E. Stutzmann, D. Griot, J.P. Montagner, and L.M. Victor, Anisotropic tomography of the Atlantic Ocean from Rayleigh surface waves, *Phys. Earth Planet. Inter., 106*, 257-273, 1998.

Silver, P.G., and W.W. Chan, Shear wave splitting and subcontinental mantle deformation, *J. Geophys. Res., 96*, 16,429-16,454, 1991.

Simons, F.K., A. Zielhuis, and R.D. van der Hilst, The deep

structure of the Australian continent from surface wave tomography, *Lithos,48*, 17-43, 1999.

Smith, M.L., and F.A. Dahlen, The azimuthal dependence of Love and Rayleigh wave propagation in a slightly anisotropic medium, *J. Geophys. Res., 78*, 3321-3333, 1973.

Stutzmann, E., and J.P. Montagner, An inverse technique for retrieving higher mode phase velocity and mantle structure, *Geophys. J. Int., 113,* 669-683, 1993.

Takeuchi, H., and M. Saito, Seismic surface waves, *Methods Comput. Phys., 11,* 217-295, 1972.

Tanimoto, T., and D.L. Anderson, Mapping convection in the mantle, *Geophys. Res. Lett., 11*, 287-290, 1984.

Tarlowski, C., P. Milligan, and T. Mackey, Magnetic anomaly map of Australia, scale 1:5 000 000, Aust. Geol. Surv. Org., Canberra , 1996.

Tong, C., O. Gudmundsson, and B.L.N. Kennett, Shear wave splitting in refracted waves returned from the upper mantle transition zone beneath northern Australia, *J. Geophys. Res., 99*, 15,783-15,797, 1994.

Trampert, J., and J.H. Woodhouse, High resolution global phase-velocity distributions, *Geophys. Res. Lett., 23*, 21-24, 1996.

van der Hilst, R., B. Kennett, D. Christie, and J. Grant, Project Skippy explores the lithosphere and mantle beneath Australia, *Eos Trans.* AGU, *75*, 177, 180-181, 1994.

van der Hilst, R.D., B.L.N. Kennett, and T. Shibutani, Upper-mantle structure beneath Australia from portable array deployment, in *Structure and Evolution of the Australian Continent, Geodyn. Ser.*, vol. 26, edited by J. Braun et al., pp. 39-57, AGU Washington, D. C. 1998.

van der Lee, S., and G. Nolet, Seismic image of the subducted trailing fragments of the Farallon plate, *Nature,386*, 266-269, 1997a.

van der Lee, S., and G. Nolet, Upper mantle *S* velocity structure of North America, *J. Geophys. Res., 102*, 22,815-22,838, 1997b.

van Heijst, H.J., and J.H. Woodhouse, Measuring surface-wave overtone phase velocities using a mode-branch stripping technique, *Geophys. J. Int., 131* 209-230, 1997.

Vinnik, L.P., L.I. Makeyeva, A. Milev, and A. Y. Usenko, Global patterns of azimuthal anisotropy and deformations in the continental mantle, *Geophys. J. Int., 111*, 433-447, 1992.

Vinnik, L.P., R.W.E. Green, and L.O. Nicolaysen, Recent deformations of the deep continental root beneath southern Africa, *Nature, 375*, 50-52, 1995.

Wellman, P., Mapping of geophysical domains in the Australian continental crust using gravity and magnetic anomalies, in *Structure and Evolution of the Australian Continent, Geodyn. Ser.*, vol. 26, edited by J. Braun et al., pp. 59-71, AGU, Washington, D. C., 1998.

Woodhouse, J.H., Surface waves in a laterally varying layered structure, *Geophys. J. R. Astron. Soc., 37*, 461-490, 1974.

Woodhouse, J.H., and A.M. Dziewonski, Mapping the upper mantle: Three-dimensional modeling of Earth structure by inversion of seismic waveform, *J. Geophys. Res., 89*, 5953-5986, 1984.

Zhang, S., and S.I. Karato, Lattice preferred orientation of olivine aggregates deformed in simple shear, *Nature, 375,* 774-777, 1995.

Zhang, Y., and T. Tanimoto, High-resolution global upper mantle structure and plate tectonics, *J. Geophys. Res.*, 98, 9793-9823, 1993.

Zielhuis, A., and G. Nolet, Shear-wave velocity variations in the upper mantle beneath central Europe, *Geophys. J. Int., 117,* 695-715, 1994a.

Zielhuis, A., and G. Nolet, Deep seismic expression of an ancient plate boundary in Europe, *Science, 265,* 79-81, 1994b.

Zielhuis, A., and R.D. van der Hilst, Upper-mantle shear velocity beneath eastern Australia from inversion of waveforms from Skippy portable arrays, *Geophys. J. Int., 127,* 1-16, 1996.

E. Debayle, Institut de Physique du Globe, CNRS and Université Louis Pasteur, 5 Rue René Descartes, F-67084 Strasbourg Cedex, France. (eric@sismo.u-strasbg.fr)

B.L.N. Kennett, Research School of Earth Sciences, Australian National University, Canberra ACT 0200, Australia. (brian@rses.anu.edu.au)

(Received April 27, 1999; revised January 24, 2000; accepted June 8, 2000.)